Hypothalamic CRH Neurons Modulate Sevoflurane Anesthesia and The Post-anesthesia Stress Responses

Shan Jiang[†], Lu Chen[†], Wei-Min Qu, Zhi-Li Huang*, Chang-Rui Chen*

Affiliations:

Department of Pharmacology, School of Basic Medical Sciences; State Key Laboratory of Medical Neurobiology and MOE Frontiers Center for Brain Science, Institutes of Brain Science, Fudan University, Shanghai, 200030, China.

*Corresponding author. E-mail: changruichen@fudan.edu.cn (C-R Chen); huangzl@fudan.edu.cn (Z-L Huang).

[†]These authors contributed equally to this work.

Acknowledgements:

We thank Prof. Gang Shu from South China Agricultural University for kindly providing CRH-Cre mice, and Yuan Meng, Mingxuan Yang, Ziheng Zhao, Yingfan Guo and Yi Zhang for assisting experiments and data analysis.

Word and Element Counts:

Abstract (140), introduction (566), discussion (1099), number of figures (7), number of tables (1), number of appendices: (number of supplemental figures: 6, number of supplemental tables: 2)

Impact statement:

Discovery of critical brain nodes explaining how sevoflurane-induced general anesthesia works and how the post-anesthesia stress responses appear.

Funding Statement:

Chang-Rui Chen, Wei-Min Qu and Zhi-Li Huang supervised the study and acquired funding. This study was supported in part by: National Major Project of China Science and Technology Innovation 2030 for Brain Science and Brain-Inspired Technology (2021ZD0203400 to Z.-L.H.), National Key Research and Development Program of China (2020YFC2005300 to W.-M.Q.), National Natural Science Foundation of China (82020108014 and 32070984 to Z.-L.H.; 82071491 and 81671317 to C.-R.C.), Shanghai Science and Technology Innovation Action Plan Laboratory Animal Research Project (201409001800), Program for Shanghai Outstanding Academic Leaders Shanghai Municipal Science and Technology Major Project and ZJLab (2018SHZDZX01).

Conflicts of Interest:

The authors declare no competing interests.

Abstract

General anesthetics benefit patients undergoing surgeries without consciousness, but the undesired stress response associated with general anesthesia (GA) causes delayed recovery and even increased morbidity in the clinic. Here, a core hypothalamic ensemble, corticotropin-releasing hormone neurons in the paraventricular nucleus of the hypothalamus (PVH^{CRH} neurons) is discovered, which regulates the anesthetic effects and post-anesthesia stress response of sevoflurane GA. Chemogenetic activation of these neurons delay the induction of and accelerated emergence from sevoflurane GA, whereas chemogenetic inhibition exert the opposite effects. Moreover, optogenetic stimulation of PVH^{CRH} neurons induce rapid cortical activation during both the steady and deep sevoflurane GA state with burst-suppression oscillations. Interestingly, chemogenetic inhibition of PVH^{CRH} neurons relieve the sevoflurane GA-elicited stress response (e.g., excessive self-grooming and elevated corticosterone level). These findings identify a common neural substrate integrating the anesthetic effect and post-anesthesia stress response of sevoflurane GA.

Keywords: general anesthesia; stress response; the paraventricular nucleus of the hypothalamus; corticotropin-releasing hormone; sevoflurane.

57 **1. Introduction**

58 In the past century, volatile general anesthetics have gained worldwide popularity in clinics
59 owing to their favorable properties, including a more pleasant odor, higher potency, low toxicity,
60 and rapid recovery [1]. As an ideal volatile anesthetic agent, sevoflurane is commonly used for
61 rapid and smooth induction and maintenance for general anesthesia (GA) [2]. However,
62 undesirable excessive stress responses of patients toward sevoflurane GA may result in
63 prolonged rehabilitation and long-term prognosis [3]. At present, the neuronal mechanisms that
64 mediate the anesthetic effects and post-anesthesia stress response of sevoflurane GA remain
65 poorly understood.

66 There is increasing evidence supporting the 'shared circuits hypothesis' of GA and sleep,
67 in which different GA drugs may exert hypnotic effect through a shared brain network with
68 wake-sleep regulation [4]. The paraventricular nucleus of the hypothalamus (PVH) is one of the
69 pivotal wake-promoting nuclei [5,6], which has dense reciprocal connections with numerous
70 neuroanatomical sites [6] that promote both wakefulness and emergence from inhaled GA,
71 including the lateral septum (LS) [7], paraventricular thalamus (PVT) [8,9], and parabrachial
72 nucleus (PB) [10-14]. The PVH mainly consists of glutamatergic neurons [15]. Specifically activating
73 PVH glutamatergic neurons using chemogenetic approaches potently enhances the proportion
74 of wakefulness, while lesions of PVH glutamatergic neurons has been shown to lead to serious
75 hypersomnia in both mice and patients [5,6]. As a subgroup of PVH glutamatergic neurons [16],
76 corticotropin-releasing hormone neurons in the PVH (PVH^{CRH}) neurons are involved in
77 hypothalamic circuitry underlying stress-induced insomnia [17]. Mild optogenetic stimulation of
78 PVH^{CRH} neurons evoked persistent wakefulness, which mimicked insomnia elicited by restraint
79 stress [17]. Collectively, this evidence suggests that PVH^{CRH} neurons may play a role in regulating
80 states of consciousness in GA.

81 The perioperative stress response is a spectrum of physiological changes occurring
82 throughout different systems in the body, including neuroendocrine, metabolic, immunological,

83 and hematological changes [18], as well as behavioral changes[19]. A prolonged stress response may
84 stimulate excess cortisol release, immunosuppression, and an increase in proteolysis, which
85 delays postoperative recovery and even leads to increased morbidity [20,21]. As an important
86 contributing factor of perioperative stress, GA-related stress has been neglected. Accumulated
87 evidence has shown that the hypothalamic-pituitary-adrenal (HPA) axis is actively involved in
88 the surgical stress during and after anesthesia [22]. Post-operatively elevated cortisol secretion is
89 considered a part of the surgical stress response [23]. Distinct from other hypnotic agents,
90 sevoflurane influences the endocrine response by increasing adrenocorticotrophic hormone and
91 cortisol levels [24,25]. Notably, PVH^{CRH} neurons serve as the initial node of the HPA axis,
92 transducing the neuronal stress signal into a glucocorticoid secretion signal [26]. Therefore, we
93 hypothesize that PVH^{CRH} neurons may act as a crucial node integrating the anesthetic effect
94 and stress response of sevoflurane GA.
95 To test our hypothesis, we first performed global screening of active neurons during the
96 post-anesthesia period in the mouse brain. We found that PVH^{CRH} neurons were preferentially
97 active during the post-anesthesia period. After observing changes in calcium signals in PVH^{CRH}
98 neurons during the induction and maintenance of, and recovery from sevoflurane GA along
99 with a robust post-anesthesia stress response, we used chemogenetic and optogenetic
100 manipulations to demonstrate how PVH^{CRH} neurons modulate sevoflurane GA. The results
101 showed that the activation of PVH^{CRH} neurons conferred resistance to sevoflurane GA.
102 Strikingly, inhibition of PVH^{CRH} neurons facilitated induction of sevoflurane GA and alleviated
103 post-anesthesia stress responses. Hence, our findings uncover a vital brain site that modulates
104 the state of consciousness as well as the stress response in sevoflurane GA.
105

106 ## 2. Results

107 ### 2.1. Identification of active neurons during the post-anesthesia period

108 Initially, to gain access to the active neurons during the post-anesthesia period, we subjected
109 the mice to either sevoflurane-oxygen anesthesia (sevo) or oxygen exposure alone (control) for
110 30 min, followed by examining the whole-brain c-fos expression 3 h later (***Figure 1A***).
111 Considering the time of the post-anesthesia stress response and the peak time of c-fos protein
112 expression (2–3 h) after neuronal activation [27], a higher level of c-fos expression was observed
113 in the PVH of sevo mice than that in control mice (***Figure 1B*** *and* ***C***). Increased staining was
114 also observed in the anterior olfactory nucleus (AON), LS, ventromedial preoptic nucleus
115 (VMPO), locus coeruleus (LC), and nucleus of the solitary tract (Sol) (***Figure 1B, C*** *and* ***Figure***
116 ***1-figure supplement 1A-C***). Interestingly, the PVH, traditionally considered a classic stress
117 center, was the brain region with the highest relative expression in the sevo group [28]. In contrast,
118 other stress-related brain regions, such as the nucleus accumbens, the ventral tegmental area,
119 and the central amygdaloid nucleus, did not exhibit robust c-fos expression (***Figure 1-figure***
120 ***supplement 2A-D***). Additionally, the medioventral periolivary nucleus (MVPO) showed
121 decreased c-fos levels after inhalation of sevoflurane (***Figure 1B*** *and* ***Figure 1-figure***
122 ***supplement 1C***). To confirm specific markers for the c-fos-positive neurons in the PVH, we
123 labelled PVH^{CRH} neurons by injecting a Cre-dependent a deno-associated virus (AAV)
124 expressing mCherry into the PVH of CRH-Cre mice because CRH staining requires special
125 pre-treatment (see Experimental Section), and found that mCherry neurons shown high
126 proportion of CRH immunoreactivity in the PVH (***Figure 1D top panel***). As shown by the
127 colocalization of c-fos and CRH signals, approximately 65.71% of activated PVH neurons were
128 CRH neurons, and approximately 73.91% of CRH neurons in the PVH were activated after
129 exposure to sevoflurane GA (***Figure 1D bottom panel, E***). These results indicate that
130 sevoflurane GA elicits robust activation of PVH^{CRH} neurons *in vivo*.

131 **2.2. Population activity of PVH^{CRH} neurons in response to sevoflurane GA**

132 To reveal the real-time responses of PVH^{CRH} neurons to sevoflurane GA, we monitored the
133 temporal dynamics of PVH^{CRH} neuronal activity in CRH-Cre mice during the whole process of
134 sevoflurane GA (i.e., induction, maintenance, emergence, and recovery phases) using *in vivo*
135 fiber photometry. A Cre-dependent AAV expressing the fluorescent calcium indicator,
136 jGCaMP7b (AAV2/9-hSyn-DIO-jGCaMP7b-WPRE-pA), was injected into the PVH of CRH-
137 Cre mice (***Figure 2A***). The expression of the virus is shown in ***Figure 2B***. During the whole
138 experimental process, the mice were placed in a vertical cylindrical cage for sevoflurane GA
139 (***Figure 2C***). As shown in ***Figure 2D***, the neural activity declined with exposure to sevoflurane
140 and increased with the cessation of sevoflurane inhalation. In detail, compared to the awake
141 baseline, PVH^{CRH} neurons showed significantly decreased neuronal activity during the 30-min
142 exposure to 1.6% sevoflurane. By analyzing the Ca^{2+} signals over four periods: pre (–30 to 0
143 min), during (anesthesia period, 0 to 30 min), post 1 (30 min to time to recovery of righting
144 reflex [RORR]), and post 2 (RORR to baseline), we found that the population activities of
145 PVH^{CRH} neurons were significantly blunted by sevoflurane exposure (during versus pre: –31.11%
146 ± 9.11%; $p = 0.027$) and gradually returned during the recovery period (post 1 versus during:
147 5.84% ± 1.19%; $p = 0.651$). These findings suggest that the activities of PVH^{CRH} neurons were
148 altered across distinct concentrations of sevoflurane.

149 Notably, PVH^{CRH} neurons exhibited higher Ca^{2+} signals compared to the awake baseline
150 after a 30-min cessation of sevoflurane inhalation. After comparing the Ca^{2+} signals of the
151 awake baseline period (pre) and post-firing period (post 2), we found that the population
152 activities of PVH^{CRH} neurons increased potently after 1.6% sevoflurane exposure (***Figure 2E***,
153 pre versus post 2: 40.38% ± 4.75%; $p = 0.002$). Consistent with the *in vivo* fiber photometry
154 results, c-fos expression in the PVH also displayed a lower level during the sevoflurane GA
155 period (mice sacrificed 0.5 h after sevoflurane onset) but a higher level during the post-firing
156 period (mice sacrificed 1.5 h after sevoflurane onset) compared to baseline (***Figure 2F***).

157 Interestingly, this hyperactivity phenomenon, lasting approximately 1 h before returning to
158 baseline levels, was accompanied by enhanced self-grooming (***Figure 2G***), which is considered
159 a stress-related behavior [29]. These results prompted us to speculate that the hyperactivities of
160 PVH^{CRH} neurons may play a vital role in the post-anesthesia stress response.

161 **2.3. Characterizations of sevoflurane GA-induced grooming**

162 Stress in animals often results in grooming and other repetitive behaviors [30]. As these
163 displacement activities are believed to have adaptive values to stress [31,32], we employed
164 excessive self-grooming as an indicator of stress response of sevoflurane GA. Next, we
165 interrogated the characteristics of sevoflurane GA-induced grooming.

166 Considering that grooming behaviors are context-sensitive and could be reflected in their
167 sequence patterns or microstructure, we analyzed these characteristics of sevoflurane GA-
168 induced grooming. Following the termination of sevoflurane GA, mice stayed awake for
169 approximately 1.5 h, during which they exhibited robust self-grooming with increased duration
170 per bout and total time spent grooming (***Figure 3-figure supplement 3A***). Because of the
171 consistent trend, we divided the post-anesthesia period (post 2) into two sections (0–50 min
172 versus 50–100 min). Compared to the former period, the latter period showed higher
173 percentages of incorrect phase transition and interrupted bouts (see 'Experimental Section'),
174 indicating elevated stress levels (***Figure 3A*** *and* ***B***); thus, we selected the latter as the
175 representative period to investigate sevoflurane GA-induced grooming.

176 Subsequently, we compared sevoflurane GA-induced grooming with four grooming
177 models related to physical and emotional stress, including those elicited by free swimming,
178 water spray, physical attack, and body restraint (***Figure 3C***). The former two models induce
179 more physical stress by moistening the fur, while the latter two models are often considered
180 models for emotional stress [33]. In line with previous reports [31,32,34,35], the mice in these two
181 emotional stress-related groups spent a higher percentage of time paw licking, while those in
182 the two fur moistening groups spent most time in grooming the body (***Figure 3-figure***

183 ***supplement 3D*** *and* ***E***). Interestingly, for transition bouts and grooming bouts per min,
184 sevoflurane GA-induced grooming during 50–100 min was close to spontaneous grooming
185 (***Figure 3E-G***), but it shared no similarities with these four grooming models in terms of the
186 mean bout duration (***Figure 3D*** *and* ***G***). A plot of the number of times spent grooming different
187 body regions also showed no similarity among sevoflurane GA-induced grooming and other
188 models (***Figure 3H*** *and* ***Figure 3-figure supplement 3D-F***). The combination of these
189 parameters suggested a low level of stress at the beginning of the post-anesthesia period
190 followed by a higher and unique level of stress with different parameters (longest mean bout
191 duration, lowest bout frequency, and average distribution of grooming time spent grooming
192 different body parts).

193 **2.4. Modulation of PVH^{CRH} neurons altered the induction and emergence of sevoflurane**
194 **GA**

195 To investigate the role of PVH^{CRH} neurons during sevoflurane GA, we micro-injected AAV-
196 DIO-hM3Dq-mCherry or AAV-DIO-hM4Di-mCherry or AAV-DIO-mCherry into the bilateral
197 PVH of CRH-Cre mice, respectively (***Figure 4A***). The c-fos expression overlaid with hM3Dq
198 or hM4Di is shown in ***Figure 4B***. We then performed behavioral experiments to determine the
199 effect of chemogenetic activation or inhibition of PVH^{CRH} neurons on the sensitivity, induction,
200 and emergence of sevoflurane GA. First, the sensitivity of sevoflurane GA was evaluated by a
201 minimum inhaled sevoflurane concentration that evoked loss of righting reflex (LORR), which
202 is a potent behavioral indicator of the onset of GA. We found that PVH^{CRH} neuron-activated
203 mice were resistant to higher concentrations of sevoflurane than the vehicle group (***Figure 4D***),
204 whereas the PVH^{CRH} neuron-inhibited mice were more vulnerable to sevoflurane GA (***Figure***
205 ***4E***). The right-shift of the dose-response curve along with the augmentation of the 50%
206 effective concentration (EC_{50}) in the PVH^{CRH} neuron-activated mice suggested that PVH^{CRH}
207 neuron activation lowered sevoflurane sensitivity during sevoflurane induction. Conversely, the
208 left-shift of the dose-response curve combined with the decrease in EC_{50} in the PVH^{CRH} neuron-

209 inhibited mice revealed higher sevoflurane sensitivity during induction. According to the dose-
210 response curves (***Figure 4-table supplement 1***), the EC_{50} of sevoflurane in term of LORR from
211 the PVH^{CRH} neuron-activated mice (n = 10) was 1.650% versus 1.516% of the vehicle group,
212 and the EC_{50} of sevoflurane in term of RORR also increased (***Figure 4-figure supplement 4A***).
213 As for the chemogenetic inhibition experiments, the EC_{50} of the PVH^{CRH} neuron-inhibited mice
214 (n = 8) was 1.337% versus 1.500% of the vehicle mice, and the EC_{50} of sevoflurane in term of
215 RORR also reduced (***Figure 4-figure supplement 4B***). The EC_{50} of sevoflurane in term of
216 either RORR or LORR did not show significant change in control group (***Figure 4-figure***
217 ***supplement 4C*** *and* ***D***).

218 We then measured the induction time (time to LORR) and emergence time (RORR)
219 following the experiment procedure outlined in ***Figure 4C***. In the chemogenetic activation
220 experiments, clozapine-N-oxide (CNO) pre-treatment led to increased induction time after 2%
221 sevoflurane exposure (***Figure 4F***). Concomitantly, the PVH^{CRH} neuron-activated mice
222 demonstrated faster emergence from 2% sevoflurane GA (***Figure 4G***). As for the chemogenetic
223 inhibition manipulation, an obvious shortened induction time and a prolonged emergence time
224 were observed after CNO pre-treatment (***Figure 4H*** *and* ***I***). These results further imply that
225 chemogenetically activating PVH^{CRH} neurons increased resilience to sevoflurane and promoted
226 awakening from sevoflurane GA, whereas chemogenetic inhibition manipulation of PVH^{CRH}
227 neurons exerted contrary effects. To further examine the role of PVH^{CRH} neurons in sevoflurane
228 GA, we genetic ablated PVH^{CRH} neurons (***Figure 4-figure supplement 5A*** *and* ***B***) and found
229 similar effects with inhibition group in terms of dose-response curve. The EC_{50} of sevoflurane
230 in terms of LORR decreased from 1.491 to 1.358% compared with control group (***Figure 4-***
231 ***figure supplement 5C***), and lesion of PVH^{CRH} neurons decreased EC_{50} of sevoflurane on RORR
232 from 1.420 to 1.326% (***Figure 4-figure supplement 5D***). Meanwhile, genetic ablation of
233 PVH^{CRH} neurons significantly facilitated induction and slowed emergence of sevoflurane GA
234 (***Figure 4-figure supplement 5E***), which show lower induction time and longer emergence time
235 than the inhibition group (***Figure 4D*** *and* ***E***).

236 Considering the temporal limitation of chemogenetic manipulation, we next employed
237 optogenetic methods with millisecond-scale control of neuronal activities to verify the role of
238 PVH^{CRH} neurons in controlling sevoflurane GA. To this end, we stereotaxically injected AAVs
239 expressing channelrhodopsin-2 (AAV2/9-hEF1a-DIO-hChR2-mCherry-pA) or AAV-DIO-
240 mCherry into the bilateral PVH of CRH-Cre mice with optical fibers implanted (***Figure 4-***
241 ***figure supplement 6A***). We verified the expression of ChR2 and the optical fiber locations after
242 behavior experiments (***Figure 4-figure supplement 6B***). Mice were placed in the same vertical
243 cylindrical cage as the apparatus for *in vivo* fiber photometry for sevoflurane GA. Optical blue-
244 light stimulation (5 ms, 30 Hz, 20–30 mW/mm^2) was applied at the onset of induction and
245 ended until LORR or started at the end of sevoflurane inhalation and continued until RORR
246 (***Figure 4-figure supplement 6C***). We found that optical activation of PVH^{CRH} neurons
247 prominently delayed the induction process (***Figure 4-figure supplement 6D***) and accelerated
248 the recovery process (***Figure 4-figure supplement 6E***) compared to the mCherry control,
249 indicating that optical activation of PVH^{CRH} neurons could prompt the emergence from
250 sevoflurane GA.

251 **2.5. Optogenetic stimulation of PVH^{CRH} neurons induced rapid emergence from steady**
252 **sevoflurane GA state**

253 We next applied 60 s of optical blue-light stimulation (5 ms, 30 Hz, 20–30 mW/mm^2) after mice
254 had maintained LORR for 30 min during steady GA state maintained by 2% sevoflurane. At
255 this stage, the electroencephalogram (EEG) patterns of the mice were characterized by an
256 increase in low-frequency, high-amplitude activity, which resembles the EEG pattern of non-
257 rapid eye movement sleep (slow-wave sleep). The optogenetics experiments were performed in
258 the similar apparatus with partially sealed chamber in the ***Figure 2C***. Photostimulation of
259 PVH^{CRH} neurons at 30 Hz during this state reliably elicited a brain-state transition from slow-
260 wave activity to a low-amplitude, high-frequency activity in ChR2 mice, but not in mCherry
261 mice (***Figure 5A*** *and* ***B***). We also observed behavioral emergence (including body movements

262 of limbs, head, and tail, righting, and walking) (Table S2, Supporting Information) combined
263 with enhanced electromyography (EMG) activity after photostimulation at 30 Hz. Spectral
264 analysis of EEG data revealed that acute photostimulation of PVH^{CRH} neurons at 30 Hz elicited
265 a prominent decrease in delta power (60.83% ± 1.35% versus 40.23% ± 5.30%; p = 0.045;
266 ***Figure 5C** and **E***) and an increase in alpha power (7.47% ± 0.41% versus 12.42% ± 0.93%; p
267 = 0.033; ***Figure 5C** and **E***) and beta power (6.01% ± 0.245% versus 11.23% ± 1.27%; p = 0.025;
268 ***Figure 5C** and **E***). However, there was no significant difference between the EEG spectrum of
269 pre-stimulation and stimulation periods in mCherry mice (***Figure 5D and F***). These findings
270 revealed that optogenetic activation of PVH^{CRH} neurons was sufficient to induce cortical
271 activation and behavioral emergence during the steady sevoflurane GA state.

272 **2.6. Optogenetic stimulation of PVH^{CRH} neurons induced EEG activation during burst-**
273 **suppression oscillations induced by deep sevoflurane GA**

274 We further explored the role of PVH^{CRH} neurons in the regulation of deep sevoflurane GA,
275 during the burst-suppression phase, in which the EEG pattern is characterized by flat periods
276 interspersed with periods of alpha and beta activity [36]. After the maintenance of burst-
277 suppression EEG mode for at least 5 min, we delivered 60 s of optical stimulation (5 ms, 30 Hz,
278 20–30 mW/mm^2) and found that EEG activation mainly occurred with an average latency of 20
279 s and maintained for a few minutes before returning to burst-suppression mode. However, the
280 EMG activity was not significantly different between pre-/post-stimulation periods of ChR2
281 mice (***Figure 6A***) and mCherry mice (***Figure 6B***). Statistical analysis of 1 min of EEG
282 recordings (optical stimulation for 20 s and 20 s before photostimulation) demonstrated a robust
283 decline in delta power (from 53.85% ± 2.58% to 41.46% ± 2.37%, p = 0.005; ***Figure 6C** and*
284 ***E***) and an increase in theta power (from 24.25% ± 3.50 to 32.07% ± 2.12%, p = 0.017; ***Figure***
285 ***6C** and **E***), alpha power (from 6.72% ± 1.16% to 11.15% ± 1.37%, p = 0.024; ***Figure 6C** and*
286 ***E***), and beta power (from 4.00% ± 0.55% to 7.56% ± 0.01%, p = 0.026; ***Figure 6C** and **E***).
287 Besides, EEG spectrum analysis of the pre- and post-stimulation periods showed similar trends,

288 but with no significant difference between the EEG power spectrum of the two periods (***Figure***
289 ***6E***). As for the mCherry mice, 60 s of blue-light stimulation had no significant effect on either
290 EEG or EMG activity (***Figure 6B, D*** *and* ***F***). These results collectively suggested that PVH^{CRH}
291 neuronal activation was sufficient to facilitate EEG cortical activation but not to promote
292 behavioral emergence during deep states of sevoflurane GA with burst-suppression oscillations.

293 **2.7. Chemogenetic inhibition of PVH^{CRH} neurons compromised the stress response after**
294 **sevoflurane GA**

295 Given the hyperactivity of PVH^{CRH} neurons and accompanying increase in self-grooming after
296 exposure to sevoflurane GA, we investigated whether PVH^{CRH} neurons are recruited while mice
297 are subjected to post-anesthesia stress. We assessed the behavioral effect of chemogenetic
298 inactivation of these neurons via the bilateral expression of the inhibitory hM4Di receptors
299 (***Figure 7A***). Following the protocol shown in ***Figure 7B***, we found that inhalation of 1.6%
300 sevoflurane induced higher expression of c-fos in the PVH, which was significantly suppressed
301 by chemogenetic inhibition of PVH^{CRH} neurons (***Figure 7C***). Hypothalamic CRH neurons
302 control the circulating levels of corticosteroid stress hormones in the body [37]. In line with the
303 c-fos expression, serum CRH levels showed similar changes after sevoflurane inhalation both
304 with and without chemogenetic inhibition (***Figure 7D***), suggesting that peripheral CRH levels
305 changed with the same direction of PVH^{CRH} neuronal activity.

306 Considering that corticosterone (CORT) is a hormone commonly used to measure stress
307 in rodents [38], we measured the serum CORT levels and found that 30 min of 1.6% sevoflurane
308 inhalation prominently evoked increased serum CORT concentrations after 1-h termination of
309 sevoflurane compared to that in groups inhaling pure oxygen (both groups injected saline or
310 CNO), which were restored to normal levels (***Figure 7E***). However, although the serum CRH
311 levels of pure oxygen groups decreased after CNO injection, there was no significant difference
312 in serum CORT concentrations between saline and CNO injection groups after inhalation of
313 pure oxygen. These results implicate that the inhibition of PVH^{CRH} neurons lowers the high

314 levels of serum CORT due to sevoflurane exposure.

315 Next, we observed the stress-related behavior after inhaling pure oxygen (O_2) or 1.6%
316 sevoflurane (sevo) for 30 min (***Figure 7B***). Analysis of self-grooming behavior (1.5 h after
317 sevoflurane GA cessation) showed that the percentage of time spent self-grooming increased
318 after 1.6% sevoflurane exposure (***Figure 7F***). To validate the higher level of stress associated
319 with sevoflurane GA, we conducted a series of tests to measure stress levels, including the open
320 field test (OFT) (***Figure 7G***) and the elevated plus-maze test (EPM) (***Figure 7H***). Combining
321 the results of the tests confirmed that the post-anesthesia period is associated with a high level
322 of stress. To further determine the influence of chemogenetic inhibition of PVH^{CRH} neurons on
323 the post-anesthesia stress response, we also performed stress-related behavioral testing on
324 CRH-Cre mice expressing hM4Di receptors (n = 8 mice) in the PVH 30 min after i.p.
325 administration of 3 mg/kg CNO or vehicle (***Figure 7A***). We observed that after 30 min of 1.6%
326 sevoflurane exposure, mice moved shorter distances in the central area during the OFT (***Figure***
327 ***7G and I***) and spent less time in the open arms during the EPM test (***Figure 7H and I***) compared
328 to the pure oxygen inhalation group. Intriguingly, PVH^{CRH} neuron-inhibited mice showed
329 similar central distance and time spent in the open arms to those of the pure oxygen inhalation
330 group, indicating that chemogenetic inhibition of PVH^{CRH} neurons abolished the stress response
331 after sevoflurane GA.

332 **3. Discussion**

333 Here, applying cutting-edge techniques, we found that PVH^{CRH} neuronal activity decreased
334 during sevoflurane induction and gradually increased during the emergence phase, followed by
335 hyperactivities with increased stress levels in mice after termination of sevoflurane
336 administration. Furthermore, the modulation of PVH^{CRH} neurons bidirectionally altered the
337 induction and recovery of sevoflurane GA. More importantly, chemogenetic inhibition of this
338 population attenuated the post-anesthesia stress response, supporting the role of PVH^{CRH}

339 neurons in mediating states of consciousness and stress response associated with sevoflurane
340 GA.

341 The reversible loss of consciousness induced by sevoflurane GA has been reported to be
342 the result of mutual regulation of numerous nuclei, including several wake-promoting
343 ensembles[39], such as dopaminergic neurons in the ventral tegmental area [40,41], glutamatergic
344 neurons in the PVT [42] and PB [10,43], and neurons expressing dopamine D1 receptors (D1R) in
345 the nucleus accumbens (NAc)[36], as well as sleep-promoting populations, such as GABAergic
346 neurons in the rostromedial tegmental nucleus [44,45]. In our study, we identified a new brain
347 region involved in sevoflurane GA - PVH^{CRH} neurons - the activation of which prolongs the
348 induction time and shortens the emergence time of sevoflurane GA. EEG is used to monitor the
349 depth of anesthesia, and the EEG activity is linked to behavioral states of GA [46]. Burst
350 suppression is a phenomenon that occurs at deep anesthesia and is caused by the interaction of
351 the hyperexcitable cortex with a refractory phase after the burst [47,48]. This hyperexcitability is
352 favored by reduced inhibition of anesthetics [47]. Notably, photostimulation of PVH^{CRH} neurons
353 effectively elicited cortical activation and behavioral emergence during steady sevoflurane GA
354 state but only caused cortical activation during burst-suppression oscillations. Compared to the
355 potent effect of optical stimulation of NAc D1R neurons during burst-suppression [36], our results
356 indicate that optogenetic activation of PVH^{CRH} neurons is insufficient to reverse the reduced
357 inhibition. Furthermore, similar to the 'Arousal-Action Model,' [49] GA-inhibiting neurons can
358 also be classified into two categories referred to as 'arousal neurons' and 'action neurons.'
359 Activation of the arousal neurons promotes EEG desynchronization but is insufficient to cause
360 EMG activation during GA. In contrast, stimulation of action neurons causes both EEG
361 desynchronization and behavioral emergence during GA. Based on this model, PVH^{CRH}
362 neurons can be classified as the arousal neurons, while NAc D1R neurons belong to the action
363 neurons. Furthermore, it has been reported that preoperative anxiety increases the anesthetic
364 requirements intraoperatively and prolongs recovery from anesthesia [50,51], indicating that stress
365 may induce abnormal neuronal activity, which influences the effect of anesthetic drugs and

366 alters the induction of and emergence from GA. Given the vital role of PVH^{CRH} neurons in the
367 stress response regulation, it is also possible that PVH^{CRH} neurons modulate sevoflurane GA
368 through influencing stress levels.

369 The postoperative stress response is commonly associated with GA combined with surgery
370 trauma. HPA activation during and after surgeries can result from multiple factors aside from
371 anesthesia, including pain, anxiety, inflammation. Effective modulation of the stress response
372 is of great importance in reducing the incidence of complications. As a predominant
373 presentation of the post-anesthesia stress response, sevoflurane-induced EA is common, with
374 an incidence of up to 80% in clinical reports, and is characterized by hyperactivity, confusion,
375 delirium, and emotional agitation [52,53]. Such responses pose the risk of neurotoxicity, delayed
376 neurological development, and even cognitive deficits. However, a broad consensus on animal
377 models mimicking this post-anesthesia stress response has yet to be established. Stress often
378 leads to grooming and other repetitive behaviors, such as digging and circling in rodents [30,54,55],
379 and self-grooming is frequently observed and believed to contribute to post-stress de-arousal
380 with adaptive value [31,32]. In this study, we observed increased self-grooming and a series of
381 other stress-related behavioral parameters during the post-anesthesia period, combined with an
382 elevated serum CORT level, strongly indicating the high stress level, and supporting these
383 measures as indicators of post-anesthesia stress responses in animal models. Of note, the
384 hyperactivity of PVH^{CRH} neurons and behavior (e.g., excessive self-grooming) in mice could
385 partly recapitulate the observed agitation and underlying mechanisms during the emergence
386 from sevoflurane GA in patients. Our findings may further help us to understand the underlying
387 mechanism related to post-anesthesia stress responses observed in patients, leading to the
388 development of strategies to prevent or treat the post-anesthesia stress response.

389 Of particular note, the PVH is canonically viewed as the key endocrine controller of the
390 stress response [56] and complex behavior after stress [57,58], including self-grooming [59]. A recent
391 study found that this role of the PVH was instructed by glutamatergic inputs from the lateral
392 hypothalamus (LH) [60]. Moreover, multiple lines of evidence have also demonstrated that

393 PVH^{CRH} neurons are not only responsible for launching the endocrine component of the
394 mammalian stress response [56] but also for orchestrating post-stress behavior, including
395 grooming [58]. For example, empirical evidence proposed that the ‘‘PVH^{CRH}-the caudal part of
396 the spinal trigeminal nucleus-spinal’’ descending pathway translates stress-related stimuli into
397 motor actions of self-grooming [61]. In our study, we observed elevated PVH^{CRH} neuronal activity
398 along with excessive self-grooming during the post-anesthesia period. Inspiringly,
399 chemogenetic inhibition of PVH^{CRH} neurons significantly alleviated these responses,
400 underscoring the crucial role of PVH^{CRH} neurons in sevoflurane GA-induced self-grooming.
401 Across the whole GA process, PVH^{CRH} neurons were greatly suppressed under sevoflurane GA
402 but were recruited to control stress responses with rebound excitation after cessation of
403 sevoflurane GA, and therefore evoked self-grooming and other behaviors to facilitate the
404 reduction in stress level. Therefore, our data contribute to an emerging view that PVH^{CRH}
405 neurons also play a key role in mediating the post-anesthesia stress responses.

406 Interestingly, we found that sevoflurane GA-induced self-grooming exhibited exclusive
407 features different from other grooming models, and the LH, which provides glutamatergic
408 inputs to the PVH in grooming [60], was not activated during the post-anesthesia period (**Figure**
409 **1-figure supplement 2B**), implying the existence of other functional pathways. PVH^{CRH}
410 neurons received direct long-range GABAergic inputs from multiple brain regions, such as the
411 LS, raphe magnus nucleus, and bed nucleus of the stria terminalis [62]. Meanwhile, it has been
412 demonstrated that the neuronal activity of the suprachiasmatic nucleus negatively regulates the
413 activity of PVH^{CRH} neurons by GABA release [63]. This evidence provides a possible explanation
414 for the hyperactivity of PVH^{CRH} neurons in the post-anesthesia period, whereby sevoflurane
415 GA suppresses activity of these brain areas, and therefore disinhibits PVH^{CRH} neurons by
416 decreasing GABAergic inputs. Further research is required to fully understand this mechanism.

417 In conclusion, we identified a pronounced node linking the anesthetic effect and post-
418 anesthesia stress response of sevoflurane GA, which offers new evidence for the neuronal
419 regulation of sevoflurane GA and provides a potential brain target for further study on the

420 modulation of the post-anesthesia stress response.

421 **4. Experimental Section**

422 **Mice**

423 CRH-Cre mice (Crh < Cre > B6(Cg)-Crh$^{tm1(cre)Zjh}$/J, JAX #012704) mice were kindly provided
424 by Prof. Gang Shu from South China Agricultural University and were obtained from the
425 Shanghai Model Organisms Center. Wild-type C57BL/6 and CD-1 mice were obtained from
426 the Experimental Animal Management Department, Institute of Family Planning Science,
427 Shanghai. Mice were group-housed in a soundproof room, with an ambient temperature of 22
428 ± 0.5°C and a relative humidity of 55% ± 5%. The mice were provided with adequate amounts
429 of food and water, and were housed under an automatic 12-h light/12-h dark cycle (illumination
430 intensity »100 lux, lights on at 07:00). Adult C57BL/6 male mice (CRH-Cre and wild-type
431 mice, 8–10 weeks old, 20–30 g) were used for all experiments; adult CD-1 male mice (4–6
432 months old, 40–50 g) were used for the direct attack-induced model. All behavioral experiments
433 were performed during the daytime (7:00–19:00). Animals were randomly divided into the
434 experimental groups and control group. CRH-Cre mice were used in calcium fiber photometry
435 recordings, chemogenetic and optogenetic manipulations, and wild-type mice were used for the
436 identification of active neurons and the characterization of self-grooming during the post-
437 anesthesia period. All experimental procedures were approved by the Animal Care and Use
438 Committee of Fudan University (certificate number: 20160225-073). All efforts were made to
439 minimize animal suffering and discomfort and to reduce the number of animals required to
440 produce reliable scientific data.

441 **Surgery**

442 Mice were anesthetized with 2% pentobarbital sodium (45 mg/kg) by intraperitoneal injection
443 and placed on a stereotaxic frame (RWD Life Science, China). The temperature of each mouse
444 was maintained constant using a heading pad during the operation. After shaving the head and
445 sterilizing with 75% ethanol, the parietal skin was cut along the sagittal suture and small

446 craniotomy holes were made above the PVH. For chemogenetic experiment, the virus
447 containing recombinant AAV-EF1α-DIO-hM3D(Gq)-mCherry-WPRE (3.3×10^{12} vector
448 genomes (VG)/mL, Brain VTA, China), or AAV2/9-hEF1α-DIO-hM4D(Gi)-mCherry-pA
449 (3.3×10^{12} VG/mL, Taitool Bioscience, China), or a viral vector encoding Cre-dependent
450 expression of Caspase-3 (AAV-CAG-FLEX-taCasp3-TEVp, 5.88×10^{12} VG/mL) was
451 bilaterally injected into the PVH (anteroposterior [AP] = –0.4–0.5 mm, mediolateral [ML] = ±
452 0.2 mm, dorsoventral [DV] = 4.5 mm deep relative to endocranium) via a glass injection needle
453 and an air-pressure-injector system at a rate of 0.1 μL/min. Control mice received injections of
454 the control virus AAV-EF1α-DIO-mCherry-WPRE-hGH pA (5.35×10^{12} VG/mL, Brain VTA,
455 China) at the same coordinates and volumes. After 7 min of injection to each site, the glass
456 pipette was left at the injection site for 8 min before slowly withdrawing.

457 For *in vivo* fiber photometry recordings and optogenetic experiments, after injecting the
458 virus (AAV2/9-hSyn-DIO-jGCaMP7b-WPRE-pA, AAV2/9-hEF1a-DIO-hChR2-mCherry-pA,
459 or AAV2/9-hEF1a-DIO-mCherry-pA, 1.61×10^{13} VG/mL, Taitool Bioscience, China) into the
460 bilateral PVH at a rate of 0.1 μL/min for 7 min, the optical fiber cannula (outer diameter [OD]
461 = 125 mm, inner diameter = 400 μm, numerical aperture [NA] = 0.37; Newdoon, Shanghai,
462 China) was placed above the unilateral PVH ([AP] = –0.4–0.5 mm, [ML] = + 0.2 mm, [DV] =
463 4.0 mm deep relative to the endocranium) before implanting the EEG and EMG electrodes. The
464 cannulas and the EEG and EMG electrodes were secured to the skull with dental cement. Mice
465 were then kept in a warm environment until they resumed normal activity and fed carefully for
466 2 weeks before the following experiments.

467 **Calcium fiber photometry recordings**

468 Using a multichannel fiber photometry system equipped with 488-nm laser (OBIS 488LS;
469 Coherent) and a dichroic mirror (MD498; Thorlabs), the fluorescence signals of the GCaMP
470 were collected by a photomultiplier tube (R3896, Hamamatsu) and recorded using a Power1401
471 digitizer and Spike2 software (CED, Cambridge, UK) with simultaneous EEG/EMG recordings.

472 During this experiment, mice were first placed in a cylindrical acrylic glass chamber connected
473 to a sevoflurane vaporizer (VP 300; Beijing Aeonmed, China). The concentration of
474 sevoflurane was monitored by an anesthesia monitor (Vamos, Drager, China) connected to the
475 chamber. In the dose-dependent experiments, after recording the baseline signals of awake mice
476 during a 20-min adaption period, different concentrations of sevoflurane (1.2%, 1.6%, or 2.0%)
477 were continuously delivered by 1.5 L/min flow of 100% oxygen for 20 min. The group inhaling
478 100% oxygen was set as the control group. As for the observation of the Ca^{2+} signals during
479 the post-anesthesia period, the baseline signals of awake mice were recorded for 30 min before
480 30-min delivery of 1.6% of sevoflurane. After turning off the sevoflurane vaporizer, the
481 recording lasted until the Ca^{2+} signals returned to the baseline level.

482 **Chemogenetic manipulations**

483 All the chemogenetic experiments were performed between 19:00–24:00, with at least a 24-h
484 washout time. After intraperitoneally pretreating the animals with saline or 3 mg/kg of CNO
485 (C4759, LKT, USA), the mice were placed in a cylindrical acrylic glass chamber with 1.5 L/min
486 flow of 100% oxygen for 20 min for habituation. To determine the sensitivity of sevoflurane,
487 mice experienced stepwise increasing exposure to sevoflurane, initially delivered at 1.2% and
488 increased every 10 min in increments of 0.1%. The righting reflex of each animal was assessed
489 after 10 min at each concentration, ensuring both brain and chamber balance. If a mouse
490 successfully returned to the prone position twice in a row, then it was considered to have a
491 complete righting reflex. Otherwise, the righting reflex was determined not to be present. The
492 induction and emergence experiments were conducted as follows. Each mouse was
493 intraperitoneally administered saline or CNO (3 mg/kg, i.p.) 1 h before the experiment. Next,
494 30-min 2% sevoflurane was delivered with 1.5 L/min 100% oxygen after 20-min habituation.
495 Following exposure to 2% sevoflurane for 30 min, the mouse was removed from the glass
496 chamber and kept in the supine position in the indoor air. The time to induction was defined as
497 the interval between the time when the mouse was put into the glass chamber full of 2%

498 sevoflurane to the time when the mice exhibited LORR. The time to emergence was defined as
499 the interval between the time when the mouse was removed from the chamber to the time when
500 it regained the righting reflex with all four paws touching the floor. Throughout the entire
501 experimental period, an electric blanket was put under the chamber to maintain the chamber
502 temperature at 36°C.

503 **Optogenetic stimulation**

504 Optical stimulation was first performed during induction of and recovery from sevoflurane GA.
505 After recording an awake EEG/EMG baseline for 10 min (continuously inhaling pure oxygen),
506 we increased the concentration of sevoflurane in the chamber to 2.0% and applied light-pulse
507 trains (5-ms pulses at 30 Hz) simultaneously until LORR. Next, after each mouse inhaled 2.0%
508 sevoflurane for 30 min, we turned off the sevoflurane vapor and initiated acute light stimulation
509 (5-ms pulses at 30 Hz) until RORR.

510 For manipulation during the steady sevoflurane GA state, light-pulse trains (473-nm, 5-
511 ms pulses at 30 Hz for 60 s) were applied according to a previous protocol [64]. In brief, a baseline
512 EEG/EMG was recorded after habituation in the acrylic glass chamber for 10 min. Next, the
513 sevoflurane vapor was turned on and the mice were subjected to sevoflurane with an initial 2.5%
514 sevoflurane for 20min and then placed in a supine position and then the sevoflurane
515 concentration was reduced to 1.4%. If the animals showed any signs of LORR, the
516 concentration was increased by 0.1% until the LORR maintained at a constant concentration
517 for at least 20 min. . Photostimulation (5-ms pulses at 30 Hz for 60 s) was applied through a
518 laser stimulator (SEN-7103, Nihon Kohden, Japan) when EEG patterns showed characteristics
519 of steady sevoflurane GA state (low-frequency, high-amplitude activity) for at least 5 min. As
520 for the burst-suppression period, a baseline EEG/EMG was recorded during habituation in the
521 acrylic glass chamber for 10 min. Next, we delivered 2% sevoflurane with pure oxygen at a
522 speed of 1.5 L/min for induction initially. After entering a continuous and steady burst-
523 suppression oscillation mode for at least 5 min, we applied blue-light stimulation (5-ms pulses

524 at 30 Hz) for 60 s. A power meter (PM10, Coherent, USA) was used to measure the power
525 intensity of the blue light before experiments.

526 **EEG/EMG analysis**

527 SleepSign software (Kissei Comtec, Japan) was used to record and analyze all EEG/EMG
528 signals. EEG/EMG signals were magnified and filtered (EEG, 0.5–30 Hz; EMG, 20–200 Hz),
529 and were digitized at a 128 Hz sampling rate. Subsequently, fast-Fourier transformation was
530 used to calculate the EEG power spectra for successive 4 s epochs in the frequency range of 0–
531 25 Hz. EEG frequency bands (delta, 0.5–4.0 Hz; theta, 4.0–10 Hz; alpha, 10–15 Hz; beta, 15–
532 25 Hz) were established in view of previous research, and relative variations in aggregate power
533 were calculated. In the optogenetic experiments during steady sevoflurane GA state, a total of
534 120-s EEG signals were analyzed (before and during acute light stimulation). As for optogenetic
535 tests during burst-suppression oscillations, a total of EEG signals from 180-s epochs were
536 calculated (before, during, and after acute light stimulation). The BSR was calculated by the
537 percentage of suppression in the time spans of 1 minute before, during, or after photostimulation.
538 Raw EEG data recorded by SleepSign software were converted to text format for further
539 analysis of BSR using MATLAB as demonstrated previously[36]. The minimum duration of burst
540 and suppression periods was set to 0.5 s.

541 **Immunohistochemistry**

542 The immunohistochemistry test was conducted according to the previous studies [65]. To confirm
543 the correct injection sites, after finishing all related experiments, each mouse was anesthetized
544 with chloral hydrate (360 mg/kg) and then perfused intracardially with 30 mL phosphate-
545 buffered saline (PBS) followed by 30 mL 4% paraformaldehyde (PFA). The brains of the mice
546 were removed and postfixed in 4% PFA overnight and then incubated in 30% sucrose phosphate
547 buffer at 4°C until they sank. Coronal sections (30 μm) were cut on a freezing microtome
548 (CM1950, Leica, Germany), and the fluorescence of injection sites was examined to locate the
549 PVH according to the histology atlas of Paxinos and Franklin (2001, The Mouse Brain in

550 Stereotaxic Coordinates 2nd edn [San Diego, CA: Academic]) using a microscope (Fluoview
551 1200, Olympus, Japan).

552 For immunostaining of c-fos, mice were sacrificed at set time according to different
553 experiments and perfused with PBS followed by 4% PFA in 0.1-M phosphate buffer. The brain
554 was then dissected and fixed in 4% PFA at 4°C overnight. Fixed samples were sectioned into
555 30-μm coronal sections using a freezing microtome (CM1950, Leica, Germany). Brain sections
556 were washed in PBS three times (5 min each time) and incubated for 48 h with primary antibody
557 in PBST (containing 0.3% Triton X-100) on a 4°C agitator using rabbit anti-c-fos (1:8000,
558 Abcam, USA) antibody, or rabbit anti-CRF (1:800, Immunostar 20084, intracerebroventricular
559 infusion of colchicine (20 μg in 500 nL saline required) 24 h before perfusion. Next, brain
560 sections were washed in PBS three times (5 min each time) and incubated with a donkey-anti-
561 rabbit Alexa488 secondary antibody (1:1000, Abcam, USA) in PBST for 2 h at room
562 temperature. Finally, the sections were mounted on glass slides, dried, dehydrated, and cover-
563 slipped. Fluorescence images were collected with an Olympus VS120 automated slide scanner.
564 Only data from mice in whom the AAV infection and optical fiber location were confirmed
565 were included. The number of animals that were excluded because of poor virus expression or
566 misplaced optical fibers are as follow: jGCaMP7b, n = 5; hM3Dq, n = 7; hM4Di, n = 10;
567 mCherry, n = 5; ChR2, n = 12; wrong optical fiber location, n = 12.

568 **Behavior experiments**

569 **Righting reflex assessment**

570 GA was defined by the loss of the righting reflex, a widely used surrogate measure in rodents.
571 All mice were placed in the air-tight, temperature-controlled, 200 mL cylindrical chambers with
572 100% oxygen flowing at a speed of 1.5 L/min for 10 min for the sake of habitation. To
573 determine the EC_{50} of LORR, the initial concentration of sevoflurane was set at 1.0%, and the
574 concentrations were increased by 0.1% every 15min. During the last 2 min of every 15 min, the
575 chambers were rotated 180° to observe whether the righting reflex of the mice was present, and

576 the number of animals that lost their righting reflex at each concentration was recorded. To
577 determine the EC_{50} of RORR, all the mice were anesthetized with 2.0% sevoflurane for 30 min,
578 and the concentration was decreased in decrements of 0.1% until all the mice had recovered
579 their righting reflex. The number of mice that had recovered their righting reflex at each
580 concentration was counted. Mice experienced stepwise increasing and diminishing exposure to
581 sevoflurane, with 15 min taken at each step, during which and an electric blanket was used to
582 maintain the chamber temperature at 36°C. The righting reflex of each animal was assessed
583 after 15 min at each concentration, ensuring both brain and chamber balance. If a mouse
584 successfully returned to the prone position twice in a row, then it was considered to have a
585 complete righting reflex. Otherwise, the righting reflex was determined not to be present.

586 **Arousal Scoring**

587 Arousal responses were scored according to the methods of previous studies[36]. Spontaneous
588 movements of the limbs, head, and tail were scored by the movements' intensity as three levels:
589 absent (0), mild (1), or moderate (2). Righting was scored as 0 if the mouse remained LORR,
590 and 2 if the mouse recovered its righting reflex. Walking was scored as follows: 0 = no further
591 movements; 1 = crawled without raising the abdomen off the chamber bottom; and 2 = walked
592 with all four paws and the abdomen off the chamber bottom. The total score for each mouse
593 was defined as the sum of all categories during the photostimulation period.

594 **Assessment of self-grooming**

595 The behavior of the animals was recorded in a test chamber (cylindrical acrylic glass, 15-cm
596 diameter, 20-cm height) in a quiet and sound-proof room by a video camera (HIKVISION, US).
597 Mice were habituated in the test chamber for 20 min before testing. For the spontaneous
598 grooming model, the mouse was placed into the test chamber and spontaneous activities were
599 recorded over a 20-min period. For restraint stress-induced grooming, the mouse was restrained
600 in a stainless-steel tube (5-cm diameter, 10 cm length) for 20 min and then placed immediately
601 into the test chamber for 20-min video recording. For direct attack-induced grooming, a

602 C57BL/6 mouse was placed directly into the home cage of a larger and aggressive CD-1 mouse
603 for 5 min with the aggressor present [66]. Immediately afterward, the C57BL/6 mouse was placed
604 in the test chamber, and its behavior was recorded for 20 min. For water spray-induced
605 grooming [60], the mouse was sprayed with a spray bottle prefilled with sterile water (25°C)
606 directed to the face, belly, and back, before placing the mouse in the test chamber for 20 min
607 of video recording. For swimming-induced grooming, the mouse was placed into a plastic
608 cylinder filled with water at 22–26°C and allowed them to freely swim for 5 min. Excess water
609 was then removed before the animal was placed into the test chamber for video recording for
610 20 min.

611 The self-grooming behavior was manually quantified by observers blinded to the
612 experimental conditions. Self-grooming was defined as when the mouse licked its own body
613 parts, including the paws legs, tail, and genitals, or stroked its own nose, eyes, head, body, with
614 the front paws [32]. An interruption of 6 s or more separated two individual bouts [34,35]. The number
615 of grooming bouts, the mean bout duration, and the total grooming time spent in the test period
616 were evaluated. For the analysis of the patterns and microstructures of grooming behavior, the
617 time spent on grooming different body parts and the transitions between different phases were
618 calculated based on previous protocols [34,35,67]. The following scaling systems based on
619 grooming stages were used: no grooming (0), paw licking (1), nose/face/head wash (2), body
620 grooming (3), leg licking (4), and tail/genitals grooming (5). Correct transitions were defined
621 as the following progressive transitions between the grooming stages: 0–1, 1–2, 2–3, 3–4, 4–5,
622 and 5–0. Incorrect transitions were characterized by skipped (e.g., 0–5, 1–5) or reversed (e.g.,
623 3–2, 4–1, 5–2) stages. Interrupted grooming bout was considered if at least one interruption was
624 recorded during the transition.

625 **Open field test**

626 The OFT is one of the most widely used behavioral tests to evaluate anxiety-like behavior in
627 rodents [67]. In the OFT, a camera was used to record the movement of mice in a 50 x 50-cm area.

628 The middle square (30 x 30 cm) of the box was considered the central area. The entire device
629 was surrounded by 40-cm high walls and its inner surface was painted black. In a quiet and
630 sound-proof room with dim light (≈ 20 lx), a mouse was placed in the middle of the arena and
631 allowed to move freely for 10 min. An automatic video tracking system (Tracking Master V3.0,
632 Shanghai Vanbi Intelligent Technology Co., Ltd.) was used to record the ambulatory activity
633 of the mice [68]. After each test, the apparatus was wiped clean with 75% alcohol to avoid the
634 influence of the previous mouse. The total and central travel distances were quantified.

635 **Elevated plus-maze test**

636 The EPM test is commonly used to measure anxiety-like behavior in mice [67]. The device
637 consists of two open arms (20 x 6 x 0.5 cm) and two closed arms (20 x 6 x 30 cm), which lie
638 across each other with an intersection part of 6 x 6 x 0.5 cm. The open arms have insignificant
639 walls (0.5 cm) to reduce the frequency of falls, whereas the closed arms are surrounded by high
640 walls (30 cm). The whole device was 70-cm above the floor. The camera was placed above the
641 EPM in the behavioral test room. Each mouse was placed in the behavioral testing room 1 h
642 before the test for adaption. During the test, the mouse was placed in the intersection area of
643 the maze, facing an open arm. After exploring the maze freely for 5 min, the mouse was
644 removed from the EPM and returned to its home cage. The maze was cleaned with a spray
645 bottle and paper towel before testing the next mouse. An automatic video tracking system
646 (Tracking Master V3.0, Shanghai Vanbi Intelligent Technology Co., Ltd.) was used to analyze
647 the movement data of the mouse. An entry was defined when half of the mouse's body entered
648 an area.

649 **Measurement of CRH and CORT levels**

650 Mice were decapitated immediately at one hour after the mice received either saline or CNO (3
651 mg/kg, C2041, LKT) treatment, respectively. Blood was rapidly collected from the retroorbital
652 plexus of the mice subjected to sevoflurane GA or pure oxygen. Considering the circadian
653 rhythm release pattern of CORT, which has lower concentrations in the morning [69], blood

654 sampling was conducted between 8:00 and 12:00 to minimize the effect of time of day on
655 glucocorticoid levels. Blood samples were allowed to clot for 2 h at room temperature before
656 centrifugation for 15 min at 1000 ×g. Serum was removed and assayed immediately or aliquoted,
657 and samples were stored at −80°C. The concentrations of CRH and CORT in the serum were
658 detected using enzyme-linked immunosorbent assay (ELISA) kits (CSB-E14068m and CSB-
659 E07969m, CUSABIO Technology, China) according to the manufacturer's instruction.

660 **Quantification and statistical analysis**

661 All data are presented as the mean ± SD. The selection of sample sizes was based on similar
662 experiments that use chemogenetic and optogenetic methods [10,36]. Paired or unpaired two-tailed
663 Student's t-test was selected to compare the two groups. If the data did not satisfy the normal
664 distribution, further analysis was performed using Wilcoxon signed-rank tests or Mann–
665 Whitney rank-sum tests. Multiple comparisons were made using one-way repeated-measures
666 ANOVA with Tukey's post-hoc test or two-way repeated-measures ANOVA followed by
667 Sidak's post hoc comparison test. Statistical analysis was performed using GraphPad Prism 8.0
668 (GraphPad Software, USA). Full details of the statistical analyses are shown in the figure
669 legends. $p < 0.05$ was statistically significant in all cases.

670 **Author contributions**

671 Shan Jiang and Lu Chen contributed equally to this work. Shan Jiang conceived, designed, and
672 performed the experiments, as well as analyzed/interpreted the data, prepared the figures, and
673 wrote the manuscript. Lu Chen performed the experiments, analyzed/interpreted the data and
674 prepared the figures. Chang-Rui Chen and Zhi-Li Huang designed the experiments and revised
675 the manuscript. Chang-Rui Chen, Wei-Min Qu and Zhi-Li Huang supervised the study and
676 acquired funding.

Data availability statement

The data that support the findings of this study are available from the corresponding author upon reasonable request.

680 **Reference**

681 1. Robinson, D.H., and Toledo, A.H. (2012). Historical development of modern anesthesia. J Invest Surg
682 *25*, 141-149. 10.3109/08941939.2012.690328.
683 2. Brioni, J.D., Varughese, S., Ahmed, R., and Bein, B. (2017). A clinical review of inhalation anesthesia
684 with sevoflurane: from early research to emerging topics. J Anesth *31*, 764-778. 10.1007/s00540-017-
685 2375-6.
686 3. Marana, E., Russo, A., Colicci, S., Polidori, L., Bevilacqua, F., Viviani, D., and Di Stasio, E. (2013).
687 Desflurane versus sevoflurane: a comparison on stress response. Minerva Anestesiol *79*, 7-14.
688 4. Lydic, R. (1996). Reticular modulation of breathing during sleep and anesthesia. Curr Opin Pulm Med *2*,
689 474-481.
690 5. Wang, Z., Zhong, Y.H., Jiang, S., Qu, W.M., Huang, Z.L., and Chen, C.R. (2022). Case Report:
691 Dysfunction of the Paraventricular Hypothalamic Nucleus Area Induces Hypersomnia in Patients. Front
692 Neurosci *16*, 830474. 10.3389/fnins.2022.830474.
693 6. Chen, C.R., Zhong, Y.H., Jiang, S., Xu, W., Xiao, L., Wang, Z., Qu, W.M., and Huang, Z.L. (2021).
694 Dysfunctions of the paraventricular hypothalamic nucleus induce hypersomnia in mice. Elife *10*.
695 10.7554/eLife.69909.
696 7. Wang, D., Guo, Q., Zhou, Y., Xu, Z., Hu, S.W., Kong, X.X., Yu, Y.M., Yang, J.X., Zhang, H., Ding,
697 H.L., and Cao, J.L. (2021). GABAergic Neurons in the Dorsal-Intermediate Lateral Septum Regulate
698 Sleep-Wakefulness and Anesthesia in Mice. Anesthesiology *135*, 463-481.
699 10.1097/ALN.0000000000003868.
700 8. Ao, Y., Yang, B., Zhang, C., Li, S., and Xu, H. (2021). Application of quinpirole in the paraventricular
701 thalamus facilitates emergence from isoflurane anesthesia in mice. Brain Behav *11*, e01903.
702 10.1002/brb3.1903.
703 9. Ren, S., Wang, Y., Yue, F., Cheng, X., Dang, R., Qiao, Q., Sun, X., Li, X., Jiang, Q., Yao, J., et al. (2018).
704 The paraventricular thalamus is a critical thalamic area for wakefulness. Science *362*, 429-434.
705 10.1126/science.aat2512.
706 10. Wang, T.X., Xiong, B., Xu, W., Wei, H.H., Qu, W.M., Hong, Z.Y., and Huang, Z.L. (2019). Activation
707 of Parabrachial Nucleus Glutamatergic Neurons Accelerates Reanimation from Sevoflurane Anesthesia
708 in Mice. Anesthesiology *130*, 106-118. 10.1097/aln.0000000000002475.
709 11. Luo, T., Yu, S., Cai, S., Zhang, Y., Jiao, Y., Yu, T., and Yu, W. (2018). Parabrachial Neurons Promote
710 Behavior and Electroencephalographic Arousal From General Anesthesia. Front Mol Neurosci *11*, 420.
711 10.3389/fnmol.2018.00420.
712 12. Xu, Q., Wang, D.R., Dong, H., Chen, L., Lu, J., Lazarus, M., Cherasse, Y., Chen, G.H., Qu, W.M., and
713 Huang, Z.L. (2021). Medial Parabrachial Nucleus Is Essential in Controlling Wakefulness in Rats. Front
714 Neurosci *15*, 645877. 10.3389/fnins.2021.645877.
715 13. Kaur, S., Pedersen, N.P., Yokota, S., Hur, E.E., Fuller, P.M., Lazarus, M., Chamberlin, N.L., and Saper,
716 C.B. (2013). Glutamatergic signaling from the parabrachial nucleus plays a critical role in hypercapnic
717 arousal. J Neurosci *33*, 7627-7640. 10.1523/jneurosci.0173-13.2013.
718 14. Qiu, M.H., Chen, M.C., Fuller, P.M., and Lu, J. (2016). Stimulation of the Pontine Parabrachial Nucleus

719 Promotes Wakefulness via Extra-thalamic Forebrain Circuit Nodes. Curr Biol *26*, 2301-2312.
720 10.1016/j.cub.2016.07.054.
721 15. Qin, C., Li, J., and Tang, K. (2018). The Paraventricular Nucleus of the Hypothalamus: Development,
722 Function, and Human Diseases. Endocrinology *159*, 3458-3472. 10.1210/en.2018-00453.
723 16. Xu, S., Yang, H., Menon, V., Lemire, A.L., Wang, L., Henry, F.E., Turaga, S.C., and Sternson, S.M.
724 (2020). Behavioral state coding by molecularly defined paraventricular hypothalamic cell type ensembles.
725 Science *370*. 10.1126/science.abb2494.
726 17. Li, S.B., Borniger, J.C., Yamaguchi, H., Hédou, J., Gaudilliere, B., and de Lecea, L. (2020).
727 Hypothalamic circuitry underlying stress-induced insomnia and peripheral immunosuppression. Sci Adv
728 *6*. 10.1126/sciadv.abc2590.
729 18. Iwasaki, M., Edmondson, M., Sakamoto, A., and Ma, D. (2015). Anesthesia, surgical stress, and "long-
730 term" outcomes. Acta Anaesthesiol Taiwan *53*, 99-104. 10.1016/j.aat.2015.07.002.
731 19. Jöhr, M. (2002). Postanaesthesia excitation. Paediatr Anaesth *12*, 293-295. 10.1046/j.1460-
732 9592.2002.00799.x.
733 20. Huiku, M., Uutela, K., van Gils, M., Korhonen, I., Kymalainen, M., Merilainen, P., Paloheimo, M.,
734 Rantanen, M., Takala, P., Viertio-Oja, H., and Yli-Hankala, A. (2007). Assessment of surgical stress
735 during general anaesthesia. Br J Anaesth *98*, 447-455. 10.1093/bja/aem004.
736 21. Desborough, J.P. (2000). The stress response to trauma and surgery. Br J Anaesth *85*, 109-117.
737 10.1093/bja/85.1.109.
738 22. Besnier, E., Clavier, T., and Compere, V. (2017). The Hypothalamic-Pituitary-Adrenal Axis and
739 Anesthetics: A Review. Anesth Analg *124*, 1181-1189. 10.1213/ANE.0000000000001580.
740 23. Gogenur, I., Ocak, U., Altunpinar, O., Middleton, B., Skene, D.J., and Rosenberg, J. (2007). Disturbances
741 in melatonin, cortisol and core body temperature rhythms after major surgery. World J Surg *31*, 290-298.
742 10.1007/s00268-006-0256-5.
743 24. Mizutani, A., Hattori, S., Yoshitake, S., Kitano, T., and Noguchi, T. (1998). Effect of additional general
744 anesthesia with propofol, midazolam or sevoflurane on stress hormone levels in hysterectomy patients,
745 receiving epidural anesthesia. Acta Anaesthesiol Belg *49*, 133-139.
746 25. Kostopanagiotou, G., Kalimeris, K., Christodoulaki, K., Nastos, C., Papoutsidakis, N., Dima, C., Chrelias,
747 C., Pandazi, A., Mourouzis, I., and Pantos, C. (2010). The differential impact of volatile and intravenous
748 anaesthetics on stress response in the swine. Hormones (Athens) *9*, 67-75. 10.14310/horm.2002.1255.
749 26. Ramot, A., Jiang, Z., Tian, J.B., Nahum, T., Kuperman, Y., Justice, N., and Chen, A. (2017).
750 Hypothalamic CRFR1 is essential for HPA axis regulation following chronic stress. Nat Neurosci *20*,
751 385-388. 10.1038/nn.4491.
752 27. Xiu, J., Zhang, Q., Zhou, T., Zhou, T.T., Chen, Y., and Hu, H. (2014). Visualizing an emotional valence
753 map in the limbic forebrain by TAI-FISH. Nat Neurosci *17*, 1552-1559. 10.1038/nn.3813.
754 28. Godoy, L.D., Rossignoli, M.T., Delfino-Pereira, P., Garcia-Cairasco, N., and de Lima Umeoka, E.H.
755 (2018). A Comprehensive Overview on Stress Neurobiology: Basic Concepts and Clinical Implications.
756 Front Behav Neurosci *12*, 127. 10.3389/fnbeh.2018.00127.
757 29. Xu, Y., Lu, Y., Cassidy, R.M., Mangieri, L.R., Zhu, C., Huang, X., Jiang, Z., Justice, N.J., Xu, Y.,
758 Arenkiel, B.R., and Tong, Q. (2019). Identification of a neurocircuit underlying regulation of feeding by

759 stress-related emotional responses. Nat Commun *10*, 3446. 10.1038/s41467-019-11399-z.
760 30. Troisi, A. (2002). Displacement activities as a behavioral measure of stress in nonhuman primates and
761 human subjects. Stress *5*, 47-54. 10.1080/102538902900012378.
762 31. Song, C., Berridge, K.C., and Kalueff, A.V. (2016). 'Stressing' rodent self-grooming for neuroscience
763 research. Nat Rev Neurosci *17*, 591. 10.1038/nrn.2016.103.
764 32. Kalueff, A.V., Stewart, A.M., Song, C., Berridge, K.C., Graybiel, A.M., and Fentress, J.C. (2016).
765 Neurobiology of rodent self-grooming and its value for translational neuroscience. Nat Rev Neurosci *17*,
766 45-59. 10.1038/nrn.2015.8.
767 33. Dayas, C.V., Buller, K.M., Crane, J.W., Xu, Y., and Day, T.A. (2001). Stressor categorization: acute
768 physical and psychological stressors elicit distinctive recruitment patterns in the amygdala and in
769 medullary noradrenergic cell groups. Eur J Neurosci *14*, 1143-1152. 10.1046/j.0953-816x.2001.01733.x.
770 34. Kalueff, A.V., Aldridge, J.W., LaPorte, J.L., Murphy, D.L., and Tuohimaa, P. (2007). Analyzing
771 grooming microstructure in neurobehavioral experiments. Nat Protoc *2*, 2538-2544.
772 10.1038/nprot.2007.367.
773 35. Kalueff, A.V., and Tuohimaa, P. (2005). The grooming analysis algorithm discriminates between
774 different levels of anxiety in rats: potential utility for neurobehavioural stress research. J Neurosci
775 Methods *143*, 169-177. 10.1016/j.jneumeth.2004.10.001.
776 36. Bao, W.W., Xu, W., Pan, G.J., Wang, T.X., Han, Y., Qu, W.M., Li, W.X., and Huang, Z.L. (2021).
777 Nucleus accumbens neurons expressing dopamine D1 receptors modulate states of consciousness in
778 sevoflurane anesthesia. Curr Biol *31*, 1893-1902.e1895. 10.1016/j.cub.2021.02.011.
779 37. Bittar, T.P., Nair, B.B., Kim, J.S., Chandrasekera, D., Sherrington, A., and Iremonger, K.J. (2019).
780 Corticosterone mediated functional and structural plasticity in corticotropin-releasing hormone neurons.
781 Neuropharmacology *154*, 79-86. 10.1016/j.neuropharm.2019.02.017.
782 38. Gong, S., Miao, Y.L., Jiao, G.Z., Sun, M.J., Li, H., Lin, J., Luo, M.J., and Tan, J.H. (2015). Dynamics
783 and correlation of serum cortisol and corticosterone under different physiological or stressful conditions
784 in mice. PLoS One *10*, e0117503. 10.1371/journal.pone.0117503.
785 39. Bao, W.W., Jiang, S., Qu, W.M., Li, W.X., Miao, C.H., and Huang, Z.L. (2023). Understanding the neural
786 mechanisms of general anesthesia from interaction with sleep-wake state: a decade of discovery.
787 Pharmacol Rev. 10.1124/pharmrev.122.000717.
788 40. Song, Y., Chu, R., Cao, F., Wang, Y., Liu, Y., Cao, J., Guo, Y., Mi, W., and Tong, L. (2021).
789 Dopaminergic Neurons in the Ventral Tegmental-Prelimbic Pathway Promote the Emergence of Rats
790 from Sevoflurane Anesthesia. Neurosci Bull. 10.1007/s12264-021-00809-2.
791 41. Gui, H., Liu, C., He, H., Zhang, J., Chen, H., and Zhang, Y. (2021). Dopaminergic Projections From the
792 Ventral Tegmental Area to the Nucleus Accumbens Modulate Sevoflurane Anesthesia in Mice. Front
793 Cell Neurosci *15*, 671473. 10.3389/fncel.2021.671473.
794 42. Li, J.Y., Gao, S.J., Li, R.R., Wang, W., Sun, J., Zhang, L.Q., Wu, J.Y., Liu, D.Q., Zhang, P., Tian, B.,
795 and Mei, W. (2022). A neural circuit from the paraventricular thalamus to the bed nucleus of the stria
796 terminalis for the regulation of states of consciousness during sevoflurane anesthesia in mice.
797 Anesthesiology. 10.1097/ALN.0000000000004195.
798 43. Xu, W., Wang, L., Yuan, X.S., Wang, T.X., Li, W.X., Qu, W.M., Hong, Z.Y., and Huang, Z.L. (2020).

Sevoflurane depresses neurons in the medial parabrachial nucleus by potentiating postsynaptic GABAA receptors and background potassium channels. Neuropharmacology *181*, 108249. 10.1016/j.neuropharm.2020.108249.

44. Vlasov, K., Pei, J., Nehs, C.J., Guidera, J.A., Zhang, E.R., Kenny, J.D., Houle, T.T., Brenner, G.J., Taylor, N.E., and Solt, K. (2021). Activation of GABAergic Neurons in the Rostromedial Tegmental Nucleus and Other Brainstem Regions Promotes Sedation and Facilitates Sevoflurane Anesthesia in Mice. Anesth Analg *132*, e50-e55. 10.1213/ANE.0000000000005387.

45. Yang, S.R., Hu, Z.Z., Luo, Y.J., Zhao, Y.N., Sun, H.X., Yin, D., Wang, C.Y., Yan, Y.D., Wang, D.R., Yuan, X.S., et al. (2018). The rostromedial tegmental nucleus is essential for non-rapid eye movement sleep. PLoS Biol *16*, e2002909. 10.1371/journal.pbio.2002909.

46. Shalbaf, R., Behnam, H., and Jelveh Moghadam, H. (2015). Monitoring depth of anesthesia using combination of EEG measure and hemodynamic variables. Cogn Neurodyn *9*, 41-51. 10.1007/s11571-014-9295-z.

47. Ferron, J.F., Kroeger, D., Chever, O., and Amzica, F. (2009). Cortical inhibition during burst suppression induced with isoflurane anesthesia. J Neurosci *29*, 9850-9860. 10.1523/jneurosci.5176-08.2009.

48. Nguyen, G., and Postnova, S. (2021). Progress in modelling of brain dynamics during anaesthesia and the role of sleep-wake circuitry. Biochem Pharmacol *191*, 114388. 10.1016/j.bcp.2020.114388.

49. Liu, D., and Dan, Y. (2019). A Motor Theory of Sleep-Wake Control: Arousal-Action Circuit. Annu Rev Neurosci *42*, 27-46. 10.1146/annurev-neuro-080317-061813.

50. Kil, H.K., Kim, W.O., Chung, W.Y., Kim, G.H., Seo, H., and Hong, J.Y. (2012). Preoperative anxiety and pain sensitivity are independent predictors of propofol and sevoflurane requirements in general anaesthesia. Br J Anaesth *108*, 119-125. 10.1093/bja/aer305.

51. Wang, H., Yu, L., Qin, Y.J., Chen, M., Wang, X., Luo, H.Q., Cong, P.L., Wang, X.L., Cai, H.M., Zhang, A.L., et al. (2021). Restoring VTA DA neurons excitability accelerates emergence from sevoflurane general anesthesia of anxiety state. Biochem Biophys Res Commun *565*, 21-28. 10.1016/j.bbrc.2021.05.079.

52. Dahmani, S., Stany, I., Brasher, C., Lejeune, C., Bruneau, B., Wood, C., Nivoche, Y., Constant, I., and Murat, I. (2010). Pharmacological prevention of sevoflurane- and desflurane-related emergence agitation in children: a meta-analysis of published studies. Br J Anaesth *104*, 216-223. 10.1093/bja/aep376.

53. Lim, B.G., Lee, I.O., Ahn, H., Lee, D.K., Won, Y.J., Kim, H.J., and Kim, H. (2016). Comparison of the incidence of emergence agitation and emergence times between desflurane and sevoflurane anesthesia in children: A systematic review and meta-analysis. Medicine (Baltimore) *95*, e4927. 10.1097/md.0000000000004927.

54. Langen, M., Durston, S., Kas, M.J., van Engeland, H., and Staal, W.G. (2011). The neurobiology of repetitive behavior: …and men. Neurosci Biobehav Rev *35*, 356-365. 10.1016/j.neubiorev.2010.02.005.

55. Langen, M., Kas, M.J., Staal, W.G., van Engeland, H., and Durston, S. (2011). The neurobiology of repetitive behavior: of mice…. Neurosci Biobehav Rev *35*, 345-355. 10.1016/j.neubiorev.2010.02.004.

56. Denver, R.J. (2009). Structural and functional evolution of vertebrate neuroendocrine stress systems. Ann N Y Acad Sci *1163*, 1-16. 10.1111/j.1749-6632.2009.04433.x.

57. Bressers, W.M., Kruk, M.R., Van Erp, A.M., Willekens-Bramer, D.C., Haccou, P., and Meelis, E. (1995).

Time structure of self-grooming in the rat: self-facilitation and effects of hypothalamic stimulation and neuropeptides. Behav Neurosci *109*, 955-964. 10.1037//0735-7044.109.5.955.

58. Füzesi, T., Daviu, N., Wamsteeker Cusulin, J.I., Bonin, R.P., and Bains, J.S. (2016). Hypothalamic CRH neurons orchestrate complex behaviours after stress. Nat Commun *7*, 11937. 10.1038/ncomms11937.

59. Kruk, M.R., Westphal, K.G., Van Erp, A.M., van Asperen, J., Cave, B.J., Slater, E., de Koning, J., and Haller, J. (1998). The hypothalamus: cross-roads of endocrine and behavioural regulation in grooming and aggression. Neurosci Biobehav Rev *23*, 163-177. 10.1016/s0149-7634(98)00018-9.

60. Mangieri, L.R., Lu, Y., Xu, Y., Cassidy, R.M., Xu, Y., Arenkiel, B.R., and Tong, Q. (2018). A neural basis for antagonistic control of feeding and compulsive behaviors. Nat Commun *9*, 52. 10.1038/s41467-017-02534-9.

61. Xie, Z., Li, D., Cheng, X., Pei, Q., Gu, H., Tao, T., Huang, M., Shang, C., Geng, D., Zhao, M., et al. (2021). A brain-to-spinal sensorimotor loop for repetitive self-grooming. Neuron. 10.1016/j.neuron.2021.11.028.

62. Yuan, Y., Wu, W., Chen, M., Cai, F., Fan, C., Shen, W., Sun, W., and Hu, J. (2019). Reward Inhibits Paraventricular CRH Neurons to Relieve Stress. Curr Biol *29*, 1243-1251.e1244. 10.1016/j.cub.2019.02.048.

63. Ono, D., Mukai, Y., Hung, C.J., Chowdhury, S., Sugiyama, T., and Yamanaka, A. (2020). The mammalian circadian pacemaker regulates wakefulness via CRF neurons in the paraventricular nucleus of the hypothalamus. Sci Adv *6*. 10.1126/sciadv.abd0384.

64. Taylor, N.E., Van Dort, C.J., Kenny, J.D., Pei, J., Guidera, J.A., Vlasov, K.Y., Lee, J.T., Boyden, E.S., Brown, E.N., and Solt, K. (2016). Optogenetic activation of dopamine neurons in the ventral tegmental area induces reanimation from general anesthesia. Proc Natl Acad Sci U S A *113*, 12826-12831. 10.1073/pnas.1614340113.

65. Luo, Y.J., Li, Y.D., Wang, L., Yang, S.R., Yuan, X.S., Wang, J., Cherasse, Y., Lazarus, M., Chen, J.F., Qu, W.M., and Huang, Z.L. (2018). Nucleus accumbens controls wakefulness by a subpopulation of neurons expressing dopamine D(1) receptors. Nat Commun *9*, 1576. 10.1038/s41467-018-03889-3.

66. Golden, S.A., Covington, H.E., 3rd, Berton, O., and Russo, S.J. (2011). A standardized protocol for repeated social defeat stress in mice. Nat Protoc *6*, 1183-1191. 10.1038/nprot.2011.361.

67. Mu, M.D., Geng, H.Y., Rong, K.L., Peng, R.C., Wang, S.T., Geng, L.T., Qian, Z.M., Yung, W.H., and Ke, Y. (2020). A limbic circuitry involved in emotional stress-induced grooming. Nat Commun *11*, 2261. 10.1038/s41467-020-16203-x.

68. Zhong, Y.H., Jiang, S., Qu, W.M., Zhang, W., Huang, Z.L., and Chen, C.R. (2021). Saikosaponin a promotes sleep by decreasing neuronal activities in the lateral hypothalamus. J Sleep Res, e13484. 10.1111/jsr.13484.

69. Kim, J.Y., Kang, H.H., Ahn, J.H., and Chung, J.W. (2008). Circadian changes in serum corticosterone levels affect hearing in mice exposed to noise. Neuroreport *19*, 1373-1376. 10.1097/WNR.0b013e32830e4c1d.

878 **Figures**

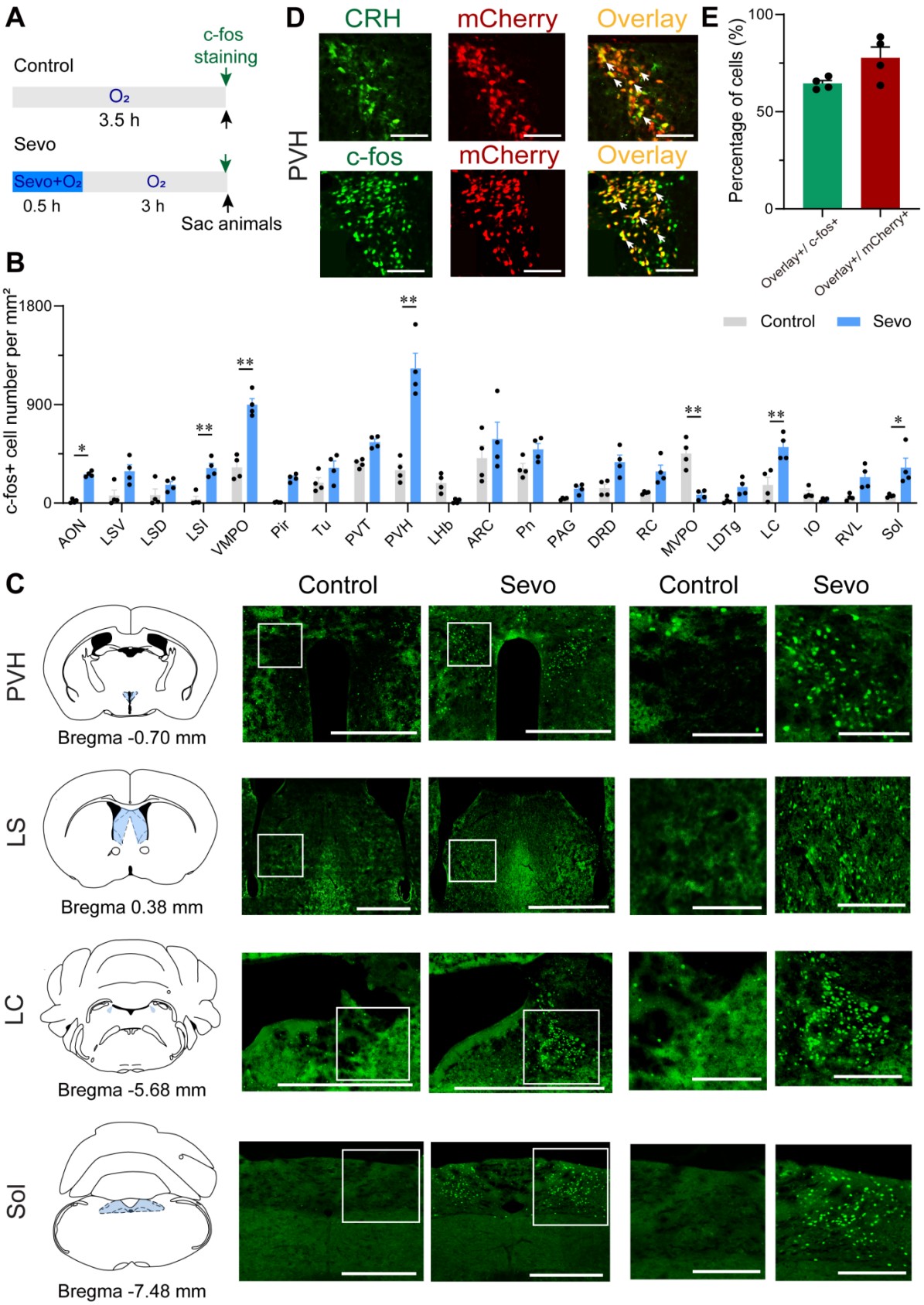
A
Control
c-fos staining
O₂
3.5 h
Sevo
Sevo+O₂
O₂
0.5 h
3 h
Sac animals
D
CRH
mCherry
Overlay
PVH
c-fos
mCherry
Overlay
E
Percentage of cells (%)
100
50
0
Overlay+/ c-fos+
Overlay+/ mCherry+
B
c-fos+ cell number per mm²
1800
900
0
Control
Sevo
AON
LSV
LSD
LSI
VMPO
Pir
Tu
PVT
PVH
LHb
ARC
Pn
PAG
DRD
RC
MVPO
LDTg
LC
IO
RVL
Sol
C
Control
Sevo
Control
Sevo
PVH
Bregma -0.70 mm
LS
Bregma 0.38 mm
LC
Bregma -5.68 mm
Sol
Bregma -7.48 mm

879

880 **Figure 1. Whole-brain mapping of active neurons during the post-anesthesia period. A.**
881 Protocol for c-fos staining. Animals were exposed to sevoflurane or oxygen for 30 min and
882 were sacrificed 3 h after the treatment. **B.** Quantification of the number of c-fos+ cells per mm^2
883 in different brain regions (n = 4, unpaired two-tailed *t*-test, $*p < 0.05$, $**p < 0.01$). AON,
884 anterior olfactory nucleus; ARC, arcuate hypothalamic nucleus; DRD, dorsal raphe nucleus,
885 dorsal part; IO, inferior olive; LC, locus coeruleus; LDTg, laterodorsal tegmental nucleus; LHb,
886 lateral habenular nucleus; LSD, lateral septal nucleus, dorsal part; LSI, lateral septal nucleus,
887 intermediate part; LSV, lateral septal nucleus, ventral part; MVPO, medioventral periolivary
888 nucleus; PAG, periaqueductal gray; Pir, piriform cortex; Pn, pontine nuclei; PVH,
889 paraventricular nucleus of the hypothalamus; PVT, paraventricular thalamus; RC, raphe cap;
890 RVL, rostroventrolateral reticular nucleus; Sol, nucleus of the solitary tract; Tu, olfactory
891 tubercle; VMPO, ventromedial preoptic nucleus. **C.** Representative images of c-fos staining in
892 the PVH, LS, LC, and Sol for a control and an experimental animal exposed to sevoflurane GA.
893 Scale bar, 500 μm (left), 250 μm (right, enlarged). **D.** Representative images showing
894 colocalization of CRH immunoreactivity and mCherry expression (upper panel, scale bar =
895 100 μm), c-fos and mCherry expression (bottom panel, scale bar = 100 μm) in the PVH of CRH-
896 Cre mice. Arrowheads indicate co-labeled neurons. **E.** Quantification of the percentage of
897 mCherry+ cells in the c-fos+ population (green) and the percentage of c-fos+ cells in the
898 mCherry+ population (red) in the PVH.
899

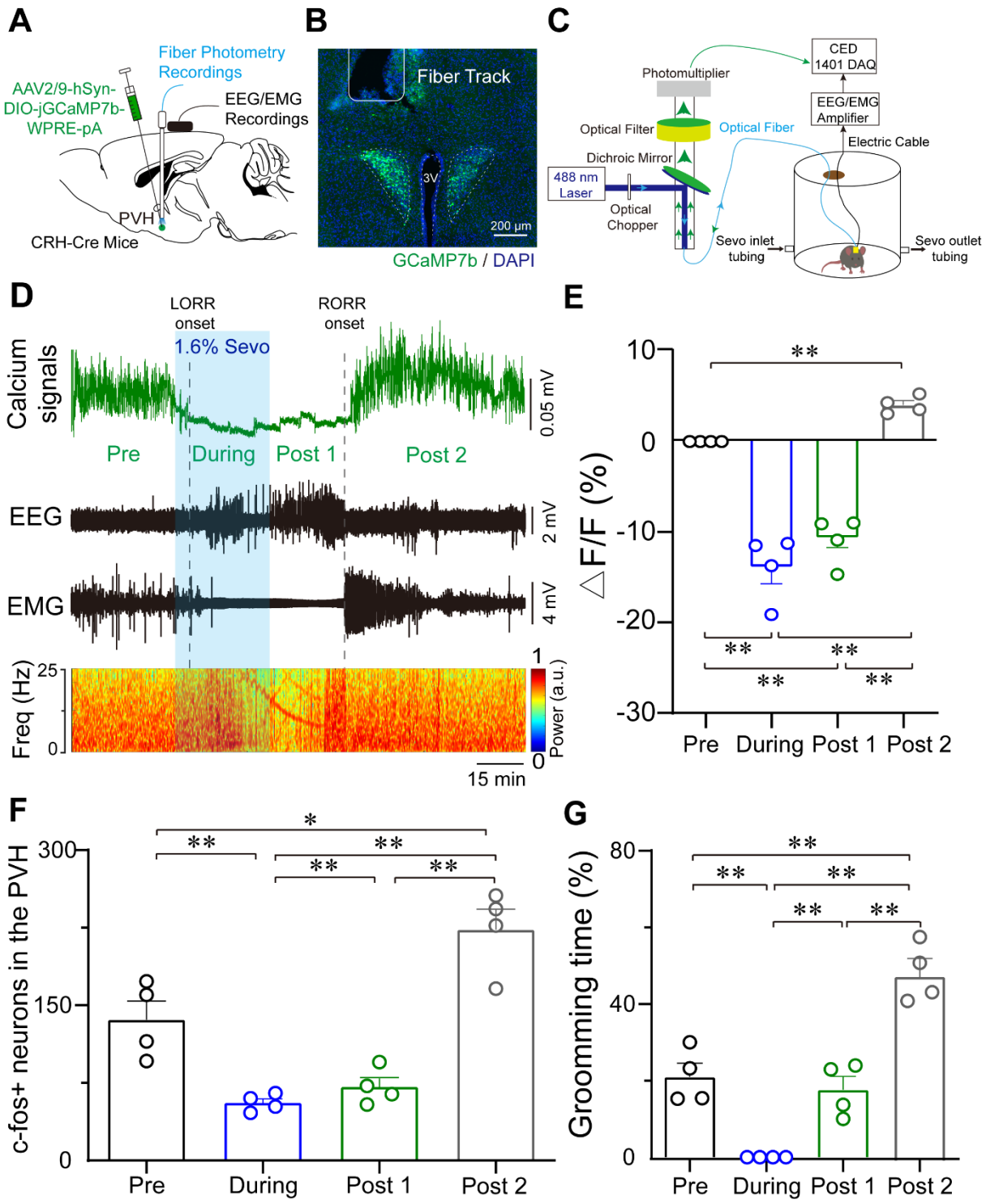

Figure 2. Population activities of PVH^{CRH} neurons in response to sevoflurane GA. A. Diagram of the virus injection, EEG/EMG electrode, and optic fiber implantation sites of CRH-Cre mice. **B.** jGCaMP7b/DAPI immunofluorescence in CRH neurons and track of the optic

904 fiber implanted above the PVH; scale bar, 200 μm. Viral expression of jGCaMP7b and
905 placement of the fiber-optic probe above the PVH. **C.** Schematic of the recording configuration.
906 **D-E.** Time courses of Ca^{2+} signals following sevoflurane anesthesia **D** and quantification of
907 Ca^{2+} signal changes before, during, and after (post 1 and post 2 periods) sevoflurane inhalation
908 (**E**, n = 4, F (3, 12) = 61.49, $p < 0.001$, one-way ANOVA with Tukey's post-hoc test; pre vs.
909 during, pre vs. post 1, during vs. post 2, post 1 vs. post 2, $p^{**} < 0.001$; pre vs. prolonged, $p =$
910 0.0894; during vs. post, $p = 0.2012$). Freq, frequency; LORR, loss of right reflexing; RORR,
911 recovery of right reflexing; Sevo, sevoflurane. **F.** Quantification of the number of c-fos+
912 neurons in the PVH before, during and after (post 1 and post 2 periods) sevoflurane inhalation
913 (n = 4, F (3, 12) = 28.15, $p < 0.001$, one-way ANOVA with Tukey's post-hoc test; pre vs. during,
914 $p = 0.0089$; pre vs. post, $p = 0.0339$; pre vs. post 2, $p = 0.0050$; during vs. post, $p = 0.8688$;
915 during vs. post 2, post 1 vs. post 2, $p^{**} < 0.001$). **G.** Time percentage of self-grooming before,
916 during, and after (post 1 and post 2 periods) sevoflurane inhalation (n = 4, F (3, 12) = 76.87, p
917 < 0.001, one-way repeated measures ANOVA with Tukey's post-hoc test; pre vs. during, pre
918 vs. post 1, $p = 0.0005$; pre vs. post 2 during vs. post 2, post 1 vs. post 2, $p^{**} < 0.0001$; during
919 vs. post 1, $p > 0.9999$).
920

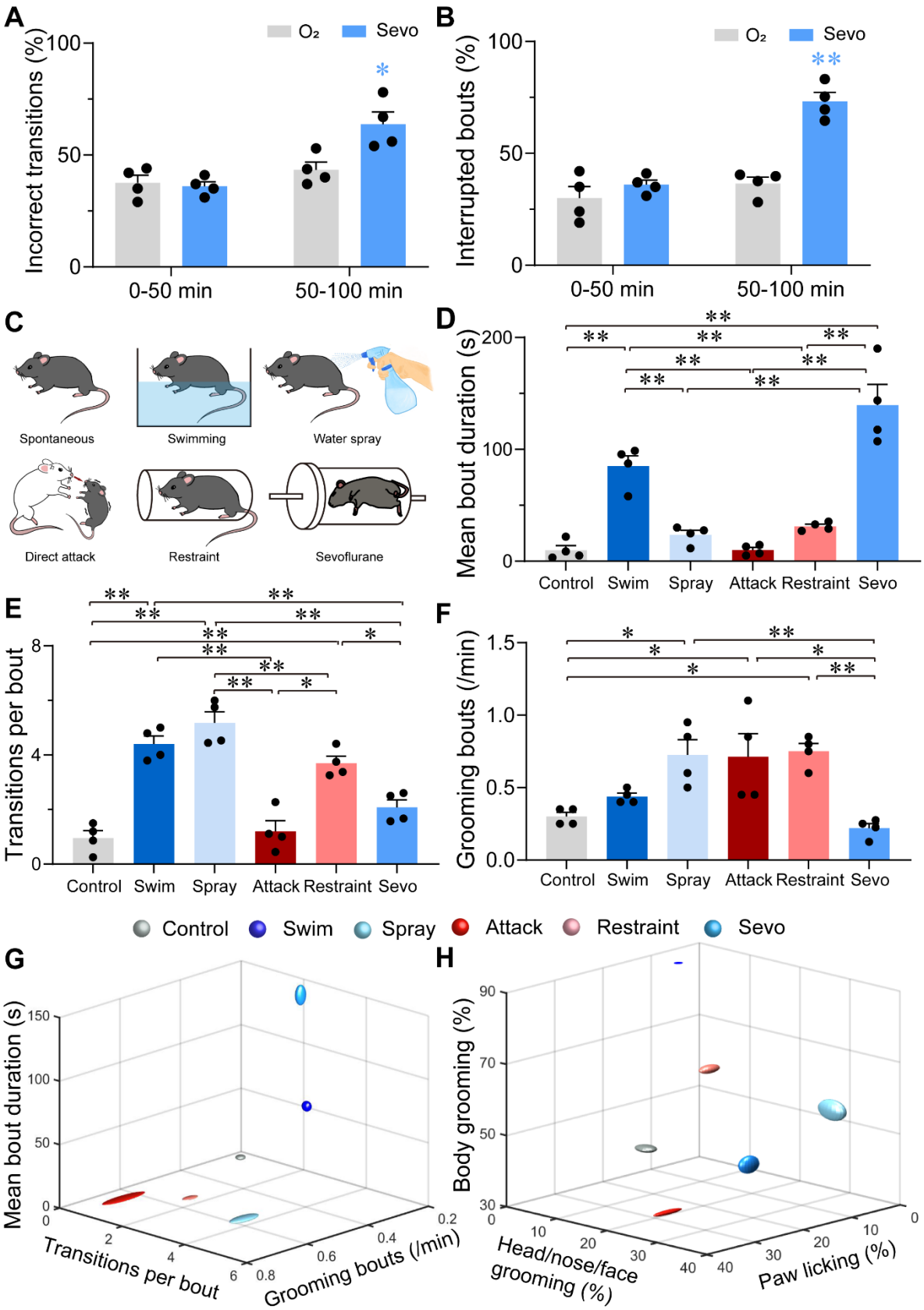
A
Incorrect transitions (%)
O₂
Sevo
0-50 min
50-100 min
B
Interrupted bouts (%)
C
Spontaneous
Swimming
Water spray
Direct attack
Restraint
Sevoflurane
D
Mean bout duration (s)
Control
Swim
Spray
Attack
Restraint
Sevo
E
Transitions per bout
F
Grooming bouts (/min)
G
Mean bout duration (s)
Transitions per bout
Grooming bouts (/min)
H
Body grooming (%)
Head/nose/face grooming (%)
Paw licking (%)

921

922 **Figure 3. Characterizations of sevoflurane GA-induced grooming. A.** Quantification of
923 incorrect transitions with respect to the cephalocaudal sequence of stereotypic grooming
924 patterns in the post-anesthesia period (n = 4, two-way ANOVAs followed by Sidak's test, F (1,
925 6) = 8.646, $p = 0.0259$, 0–50 min: O_2 vs sevo, $p = 0.9545$; 50–100 min, O_2 vs sevo, $p = 0.0055$).
926 **B.** Number of interrupted bouts in the post-anesthesia period (n = 4, two-way ANOVAs
927 followed by Sidak's test, F (1, 6) = 19.14, $p = 0.0047$, 0–50 min: O_2 vs sevo, $p = 0.4770$; 50–
928 100 min, O_2 vs sevo, $^{**}p < 0.01$). **C.** Six representative grooming models, including
929 spontaneous (control), swimming, water spray, physical attack, body restraint, and sevoflurane
930 GA-induced grooming. **D-F.** The mean bout duration (**D**, F (5, 18) = 34.52, $p < 0.0001$),
931 transitions per bout (**E**, F (5, 18) = 30.32, $p < 0.0001$), and grooming frequency (bouts per
932 min, **F**, F (5, 18) = 7.935, $p = 0.0004$) varied across the models (n = 4, one-way ANOVA with
933 Tukey's post-hoc test. $^{*}p < 0.05$; $^{**}p < 0.01$). **G-H.** 3-D plot of bout frequency, bout duration,
934 and transitions per bout (**G**); the percentage of time spent grooming different body parts (**H**).
935 The dimension of the symbol along an axis is defined by the SD of the corresponding parameter.
936

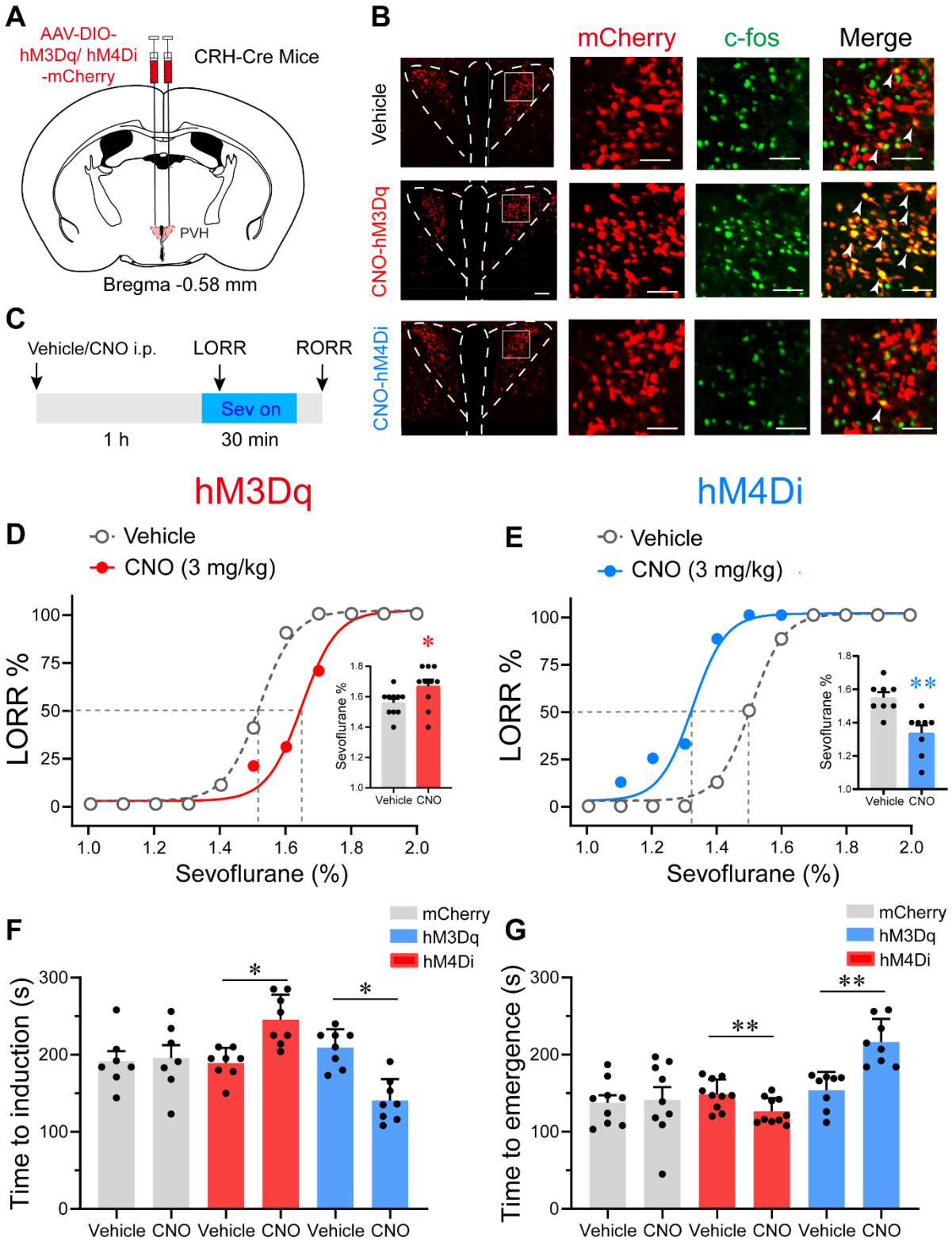

Figure 4. Chemogenetic modulation of PVH^{CRH} neurons bidirectionally altered induction

939 **of and emergence from sevoflurane GA. A.** Schematic of AAV-DIO-hM3Dq-mCherry or
940 AAV-DIO-hM4Di-mCherry or AAV-DIO-mCherry injected into the PVH of CRH-Cre mice.
941 **B.** Left: representative images of mCherry/c-fos immunofluorescence in CRH neurons after
942 vehicle or CNO treatment; scale bars, 200 μm. Right: magnified images are shown; scale bar,
943 200 μm. Arrowheads indicate co-labeled neurons. **C.** Timelines of sevoflurane anesthesia-
944 related behavioral tests measuring induction time (LORR) and emergence time (RORR). **D-E.**
945 Dose-response curves showing the percentages of mice exhibiting LORR in response to
946 incremental sevoflurane concentrations for the vehicle and CNO groups. Inset: the sevoflurane
947 concentrations at which each mouse exhibited LORR are shown (**D**, hM3Dq group, n = 10,
948 paired *t*-test, $p = 0.0411$; **E**, hM4Di group, n = 8, paired *t*-test, $p = 0.0021$). **F.** Induction time
949 with 2% sevoflurane exposure after intraperitoneal injections of vehicle or CNO for 1 h
950 (mCherry group, n = 7, paired *t*-test, $p = 0.847$; hM3Dq group, n = 10, paired *t*-test, $p = 0.0498$;
951 hM4Di group, n = 8, paired *t*-test, $p = 0.0060$). **G.** Emergence time with 2% sevoflurane
952 exposure for 1 h after intraperitoneal injections of vehicle or CNO (mCherry group, n = 7,
953 paired *t*-test, $p = 0.8298$; hM3Dq group, n = 10, paired *t*-test, $p = 0.0104$; hM4Di group, n = 8,
954 paired *t*-test, $p = 0.0099$).

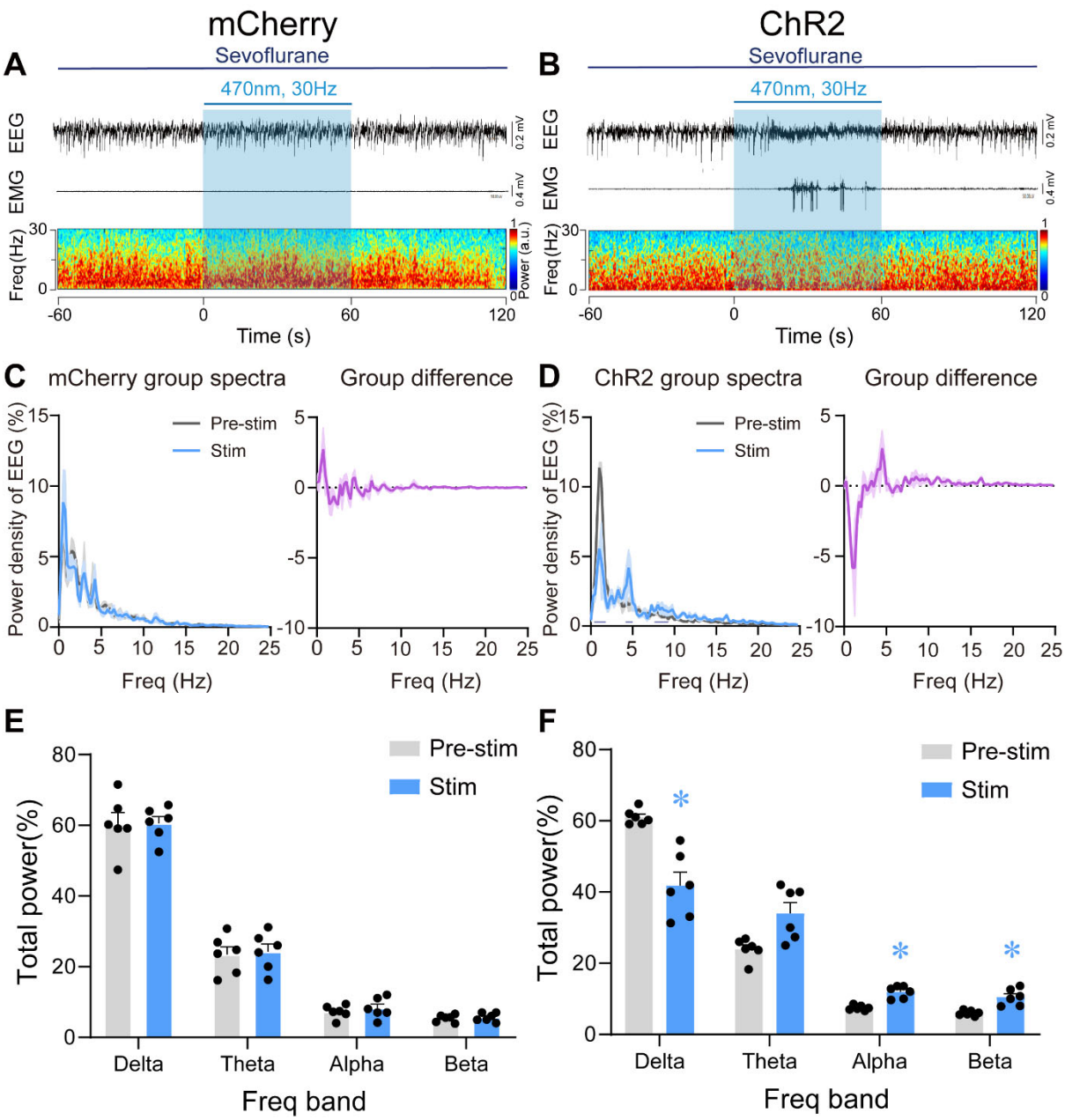

955

956 **Figure 5. Optogenetic stimulation of PVH^{CRH} neurons induced cortical activation and**
957 **behavioral emergence during continuous steady-state sevoflurane GA. A-B.** Typical
958 examples of EEG, EMG, and EEG power spectral in a mouse injected with AAV-DIO-
959 mCherry(**A**) or AAV-DIO-ChR2-mCherry (**B**) following acute photostimulation (30 Hz, 5 ms,
960 60 s) during continuous steady-state sevoflurane GA. Time 0 indicates the beginning of
961 photostimulation. The blue shadow indicates the 60-s duration of blue light stimulation. **C-D.**

962 Left: normalized group power spectral densities from PVH^{CRH}-mCherry (**C**) or PVH^{CRH}-ChR2
963 (**D**) mice with pre photostimulation (gray) and photostimulation (blue). Dark blue lines in d
964 indicate the power band with significant difference. Right: differences between normalized
965 group power spectral densities from PVH^{CRH}-mCherry (**C**) or PVH^{CRH}-ChR2 (**D**). **E-F.** Power
966 percentage changes in cortical EEG before (gray) and during (blue) photostimulation at 30 Hz
967 in PVH^{CRH}-mCherry (**E**) or PVH^{CRH}-ChR2 mice (**F**) during continuous steady-state sevoflurane
968 GA (n = 6, two-way ANOVAs followed by Sidak's test, $*p < 0.05$).

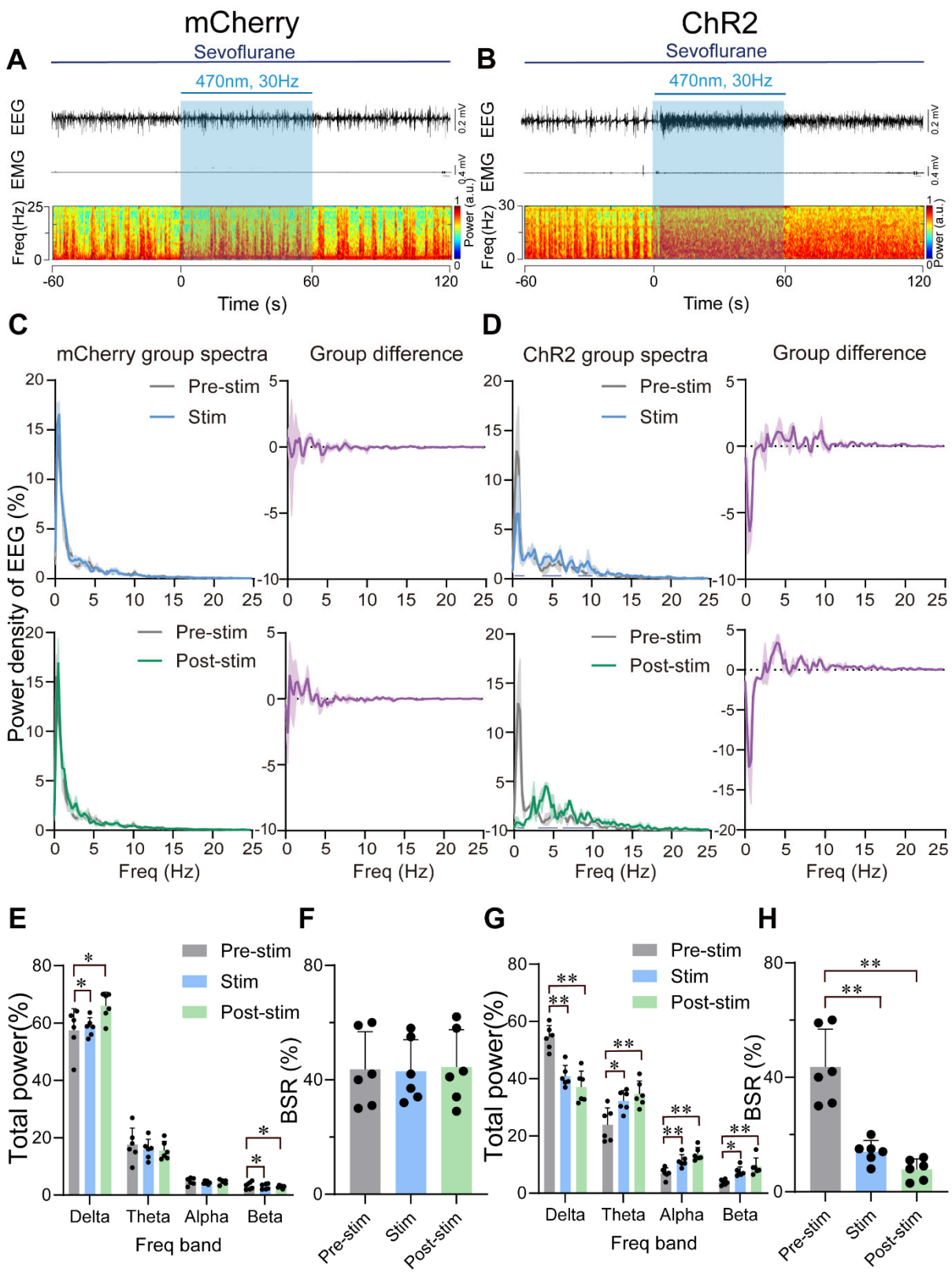

969

970 **Figure 6. Optogenetic stimulation of PVH^{CRH} neurons induced cortical activation during**

burst-suppression oscillations induced by deep sevoflurane GA. A-B. Typical examples of EEG, EMG, and EEG power spectral in a mouse injected with AAV-DIO-mCherry (**A**) or AAV-DIO-ChR2-mCherry (**B**) following acute photostimulation (30 Hz, 5 ms, 60 s) during burst-suppression oscillations. Time 0 indicates the beginning of photostimulation. The blue shadow indicates the 60-s duration of blue light stimulation. **C-D.** Top left: normalized group power spectral densities from PVH^{CRH}-mCherry mice (**C**) and PVH^{CRH}-ChR2 (**D**) with pre photostimulation (gray) and photostimulation (blue); Top right: differences between normalized group power spectral densities from PVH^{CRH}-mCherry mice (**C**) and PVH^{CRH}-ChR2 mice (**D**). Bottom left: normalized group power spectral densities from PVH^{CRH}-mCherry mice (**C**) and PVH^{CRH}-ChR2 mice (**D**) with pre photostimulation (gray) and post photostimulation (green); bottom right: differences between normalized group power spectral densities from PVH^{CRH}-mCherry mice (**C**) and PVH^{CRH}-ChR2 mice (**D**). Dark blue lines in panel d indicate the power band with significant difference. **E, G.** Power percentage changes in cortical EEG before (gray), during (blue), and post (green) photostimulation in PVH^{CRH}-mCherry (**E**) or PVH^{CRH}-ChR2 (**G**) mice during burst-suppression oscillations. **F, H.** BSR change before (gray), during (blue), and post (green) photostimulation in PVH^{CRH}-mCherry (**G**) or PVH^{CRH}-ChR2 (**H**) mice during burst-suppression oscillations (n = 6, two-way ANOVAs followed by Sidak's test, $*p < 0.05$, $**p < 0.01$). Stim, stimulation; Freq, frequency.

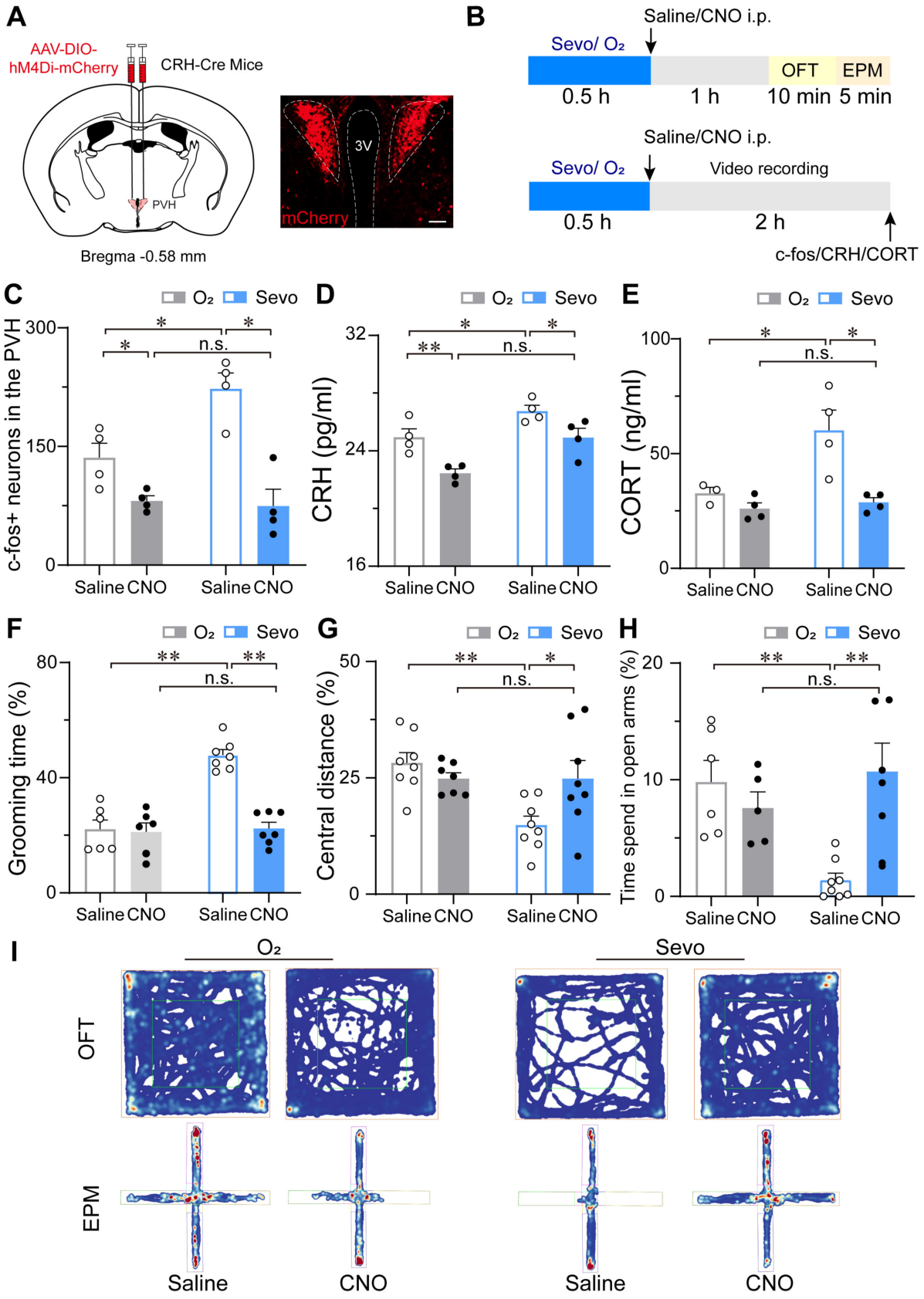
A
AAV-DIO-
hM4Di-mCherry
CRH-Cre Mice
PVH
Bregma -0.58 mm
3V
mCherry
B
Saline/CNO i.p.
Sevo/ O₂
OFT
EPM
0.5 h
1 h
10 min
5 min
Saline/CNO i.p.
Sevo/ O₂
Video recording
0.5 h
2 h
c-fos/CRH/CORT
C
O₂
Sevo
c-fos+ neurons in the PVH
n.s.
Saline CNO
Saline CNO
D
CRH (pg/ml)
E
CORT (ng/ml)
F
Grooming time (%)
G
Central distance (%)
H
Time spend in open arms (%)
I
OFT
EPM
Saline
CNO
Saline
CNO

991

992 **Figure 7. Chemogenetic inhibition of PVH^{CRH} neurons alleviated the stress response after**
993 **sevoflurane GA. A.** Schedule of sacrificing mice for c-fos quantification, collecting blood
994 samples from mice subjected to sevoflurane or pure oxygen for CRH, and CORT measurement
995 and behavior testing (OFT and EPM). **B.** The schedule of the video recording after inhalation
996 of sevoflurane or pure oxygen for 30 min. **C.** Quantification of the number of c-fos-positive
997 neurons in the PVH (n = 4, F (1, 6) = 14.62, saline: O_2 vs. sevo, $p = 0.0017$; CNO: O_2 vs. sevo,
998 $p = 0.7122$). **D-E.** Serum CRH (**D**, n = 4, F (1, 6) = 0.4513, $p = 0.5267$, saline: O_2 vs. sevo, $p =$
999 0.0456; CNO: O_2 vs. sevo, $p = 0.0077$) and CORT (**E**, n = 4, F (1, 11) = 5.691, saline: O_2 vs.
1000 sevo, $p = 0.0082$; CNO: saline: O_2 vs. sevo, $p = 0.9144$) levels following the protocol in (a). **F-**
1001 **H.** Time percentage of self-grooming (**F**, n = 8, F (1, 10) = 24.61, saline: O_2 vs. sevo, $p < 0.001$;
1002 CNO: O_2 vs. sevo, $p = 0.9275$), moving distances in the central areas of OFT (**G**, n = 8, F (1,
1003 13) = 6.953, saline: O_2 vs. sevo, $p = 0.0018$; CNO: O_2 vs. sevo, $p > 0.9999$) and time percentage
1004 of staying in the open arms of the EPM (**H**, n = 8, F (1, 7) = 12.70, saline: O_2 vs. sevo, $p =$
1005 0.0017; CNO: O_2 vs. sevo, $p = 0.3783$) after inhalation of sevoflurane or pure oxygen and
1006 administration of saline or CNO. Statistical comparisons were conducted using two-way
1007 ANOVA followed by Sidak's tests. *$p < 0.05$, **$p < 0.01$, n.s., no significant differences). **I.**
1008 Representative heatmaps of OFT and EPM after inhalation of sevoflurane or pure oxygen and
1009 administration of saline or CNO.